

Ferrocene Bioconjugates

Mojca Čakić Semenčić, Lidija Barišić*

Department of Chemistry and Biochemistry, Faculty of Food Technology and Biotechnology, University of Zagreb, Pierottijeva 6, HR-10000, Zagreb, Croatia

* Corresponding author's e-mail address: lidija.barisic@pbf.hr

RECEIVED: October 19, 2017 * REVISED: March 12, 2018 * ACCEPTED: March 26, 2018

THIS PAPER IS DEDICATED TO PROF. MLADEN ŽINIĆ ON THE OCCASION OF HIS 70TH BIRTHDAY

Abstract: In this review we present our recent contribution to the field of bioorganometallic chemistry of ferrocene. Ferrocene conjugates with biomolecules have been synthesized and characterized using IR and NMR (¹H, ¹³C, COSY, NOESY, HMBC) spectroscopy, ESI-MS and HRMS. The bioconjugates of ferrocene with resveratrol (**2**) and mannose (**10**, **11**, **14** and **15**) were biologically evaluated for their potential inhibitory effect on HepG2 cancer cells (**2**) and E. coli adherence to the bladder epithelium (**10**, **11**, **14** and **15**). The oxalamide-bridged ferrocene **17** was subjected to conformational analysis in solution and in the solid state, and tested for its gelation and cytotoxic activity. The mono- (**30–32**, **36–38**, **42–45**) and disubstituted ferrocene conjugates with natural amino acids (**21–28**, **33–35**, **39–41**, **48**, **49**, **62–65**, **69–72**) were subjected to the detailed conformational and DFT analyses in order to determine the turn-inducing potential of ferrocene scaffolds in the corresponding peptidomimetics.

Keywords: ferrocene, resveratrol, mannose, oxalamide, peptide, cytotoxic activity, hemagglutination, gelation, conformational analysis, peptidomimetics.

INTRODUCTION

FERROCENE was serendipitously discovered 66 years ago when Pauson and Kealy tried unsuccessfully to prepare fulvalene (C₁₀H₈) by reaction of cyclopentadiene bromide with iron (II) chloride. Instead of fulvalene, they obtained the orange solid that was consistent with molecular formula FeC₁₀H₁₀.^[1] A year later, Wilkinson and Woodward^[2] deduced the real structure of the novel compound - [Fe(C₅H₅)₂] - where two anionic cyclopentadienyl (Cp) rings donate 6 π electrons to the Fe²⁺ cation sandwiched between them. Since its reactivity resembles that of benzene, the name ferrocene for the novel sandwich complex was coined.^[3,4] It soon became apparent that ferrocene features several types of remarkable properties: solubility in common organic solvents, stability up to 400 °C, reactivity as a superaromatic electrophile and mild and reversible oxidation around +0.4 V vs. saturated calomel electrode (SCE) (Figure 1).

So far, ferrocenes have been reported in more than 18000 papers (Web of Science)^[5] and as such are recognized as an icon of organometallic chemistry. The recently published microreview on ferrocenes^[5] gives an

overview of ferrocene applications in fields such as nanomedicine, biological sensing (the detection of glucose in blood,^[6] protein and DNA binding, immunoassay tracers,^[7] etc.), catalysis, battery and other materials, and other areas involving supramolecular, macromolecular, and optoelectronic property aspects.

Owing to their exceptional characteristics (stability in biological media, redox activity, easy penetration through cell membrane owing to the lipophilicity, low toxicity, feasibility to chemical modification, commercial

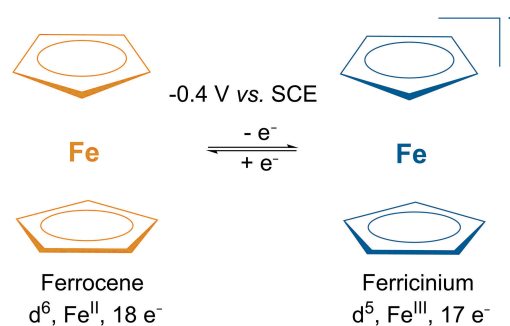


Figure 1. Reversible oxidation of ferrocene to the ferricinium ion.

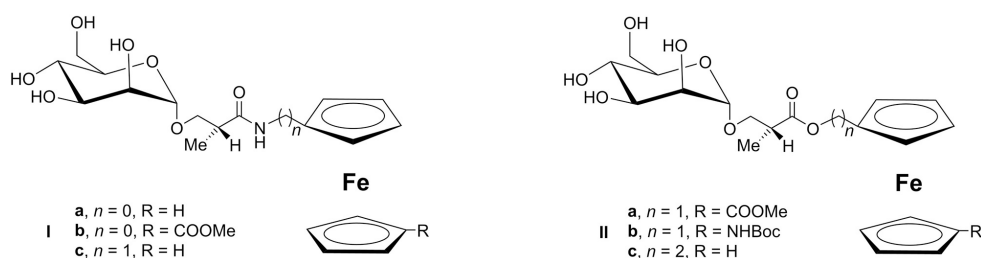


Figure 2. The mannose-containing ferrocenes I and II.

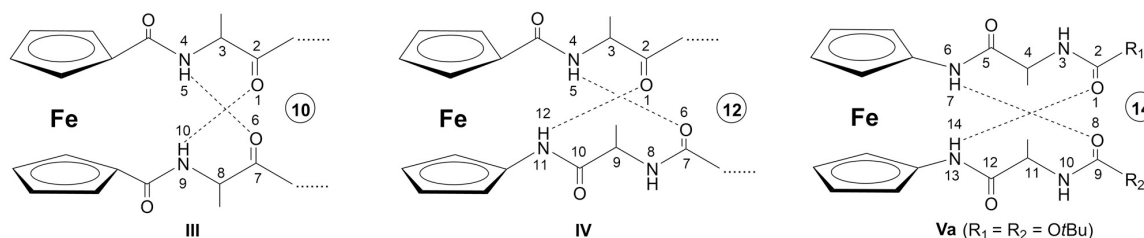


Figure 3. The bioorganometallics III, IV and Va that contain turn-inducing ferrocene scaffolds.

availability), ferrocenes have attracted much attention in the field of medicinal organometallic chemistry termed also as bioorganometallic chemistry.^[8] Ferrocene compounds have been intensively explored for medical purposes,^[8] especially in anticancer^[9,10] and antimicrobial studies. Among numerous ferrocene compounds tested for their anticancer activity, the particular attention has been paid to antiproliferative effect of ferrocenyl tamoxifen analogue named ferrocifen, on breast cancer cells.^[11] The antitumor activity of various bioferrocenes such as ferrocenyl alkyl nucleobases,^[12] azalactone ferrocene,^[13] ferrocenyl conjugates with salts of *N*-alkylpyridinium^[14] and carbohydrate ferrocene conjugates^[15] was also examined. The initial researches of antimicrobial effects of ferrocenes began with ferrocene modified penicillins, cephalosporins and rifamycin,^[16–19] and continued with derivatives containing various pharmacophore groups^[20] and structural fragments of biomolecules, such as amino acids, peptides, sugars, nucleobases and steroids.^[21,22]

Considering the biological significance of ferrocene-modified biomolecules,^[11,23–27] the joint research on the mannose inhibitors of hemagglutination **Ia–c**^[28] and **Ila–c**^[29] that contain ferrocene moiety in aglycon has been started in Rapić and Tomić groups (Figure 2). Since the urinary tract infections are mostly caused by adhesion of uropathogenic *Escherichia coli* on mannose units of a membrane glycoprotein that is expressed on superficial epithelial cells of the urinary tract,^[30] the development of antiadhesion therapeutics aimed to prevent *Escherichia coli* lectin FimH-mediated adhesion has become a focus of researches in the last 50 years. The chemical synthesis of mannose-containing antiadhesives involves the insertion of lipophilic alkyl or aromatic groups to the aglycon part,^[31] resulting in a dramatic increment of their affinity for FimH.

Therefore, the significant increment of the inhibitory activity of conjugate **Ilc** in comparison to conjugates **Ia–c** and **Ila,b** was in accordance with the enhanced inhibitory activity of the mannosides with elongated alkyl chains.^[31]

Furthermore, the conjugates of ferrocene and amino acids have been extensively studied in the field of peptidomimetics. 1,1'-Disubstituted ferrocene scaffolds, equipped with hydrogen bonding functionalities, have been employed for almost 20 years to nucleate turns and β -sheet-like structures in short peptides.^[32–37] The two cyclopentadienyl rings in ferrocene have a distance of ~ 3.3 Å which corresponds to the space between hydrogen bonding donor and acceptor sites in β -sheets. Thereby, the introduction of the peptide chains into the ferrocene scaffold brings them to adequate distance to allow their communication through intramolecular hydrogen bonding required for 3D structure formation and function of biological systems.^[38] The hydrogen bond donating/accepting properties of turn-inducing ferrocene scaffolds determine the hydrogen bonding patterning of the derived peptides: the ten-membered interstrand hydrogen-bonded rings (β -turn-like) were established in the conjugates of the amino acids or peptides with dicarbonyl-functionalized ferrocene core (**III**),^[32] the twelve-membered rings were formed in their conjugates with $-\text{NH}-\text{Fn}-\text{CO}-$ moiety (**IV**, Fn = ferrocenylene),^[33] while conjugation with diamino-functionalized ferrocene lead to the fourteen-membered hydrogen-bonded rings [also labelled as two simultaneous ten-membered rings (β -turn-like)] in the corresponding conjugates **Va**^[34] (Figure 3).

The overview of the previously reported peptides **IV** was given by Rapić.^[39]

In this contribution, the review of authors recent research results on ferrocene (bio)conjugates is given. The

first part of the paper is concerned on potential biologically active ferrocene conjugates with resveratrol and mannose. The second part of the paper is dealing with conformational behaviour of ferrocene peptidomimetics studied by means of spectroscopic methods and DFT calculations.

I. SYNTHESIS AND BIOLOGICAL EVALUATION OF FERROCENE CONJUGATES WITH RESEVERATROL AND MANNOSE

Ferrocene-resveratrol Conjugate 2

Resveratrol [3,5,4'-trihydroxystilbene (**RSV**) (Figure 4a)] is well-known to promote cardioprotection, cancer prevention and therapy, immune regulation and metabolic and neuroprotective functions.^[40–42] The approaches for improving its biological profile include modification of the number and position of the aromatic groups, insertion of a long alkyl chains or functionalized chains and the addition of acyl chains to free hydroxyl groups.^[43] Vervandier-Fasseur *et al.* applied the first approach to prepare ferrocene-containing **RSV**-derivative **VI** that was found to exhibit more than 10-fold higher inhibitory activity in primary human colon carcinoma cells (SW480) and hepatoblastoma (HepG2) cell lines compared to those of **RSV** (Figure 4b).^[44]

Encouraged by this result, we have synthesized ferrocene-**RSV** conjugate **2** equipped with trimethylene alkyl chain in order to improve its lipophilicity as a crucial

requirement for biological activity.^[45] The conjugate **2** was obtained by esterification^[46] of ferrocene butyric acid (**1**) with C3-OH group of *trans*-**RSV** in the presence of DMAP, NEt_3 and Boc_2O (Scheme 1) and its inhibitory potential on HepG2 and normal ovary cells (CHO-K1) proliferation was evaluated.

The results of cytotoxicity evaluation revealed profound effects in biological activity of ferrocene-**RSV** conjugate **2** vs. **RSV** in HepG2 cell line (Figure 5). Accordingly, IC_{50} value for **2** was 20 % lower than IC_{50} value for **RSV**. Much lower cytotoxicity on normal CHO-K1 cells was observed. In spite of the decreased activity in comparison to the previously reported conjugate **VI**^[44], our conjugate **2** was more potent than **RSV** and therefore indicated the potential for further studies on ferrocene-**RSV** conjugates that are in progress in our group.

Ferrocene-mannose Conjugates 10, 11, 14 and 15

The improved biological activity of the previously reported conjugate **IIc**^[29] was attributed to the elongation of the alkyl spacer incorporated between ferrocene core and chiral linker. Besides the elongated aglycon alkyl chain,^[47] the two structural elements - mannose moiety and hydrophobic aglycon residue - are required to achieve the antiadhesion effect. Considering these findings, we were prompted to determine if the further elongation of the alkyl chain from propyl to pentyl in bioorganometallics **10**, **11**, **14** and **15** will contribute to their pronounced inhibitory effect.^[48] The novel bioconjugates were designed to contain ester (**10**, **11**) or amide linkage (**14**, **15**) between

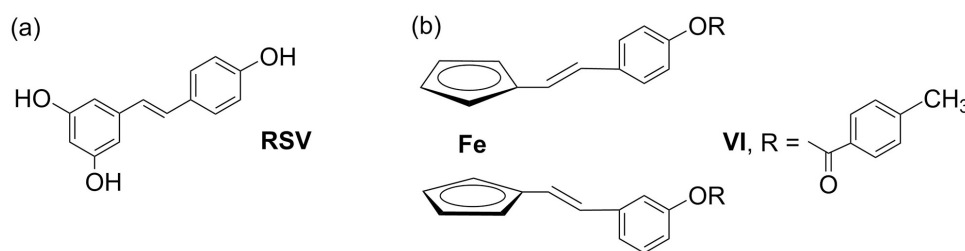
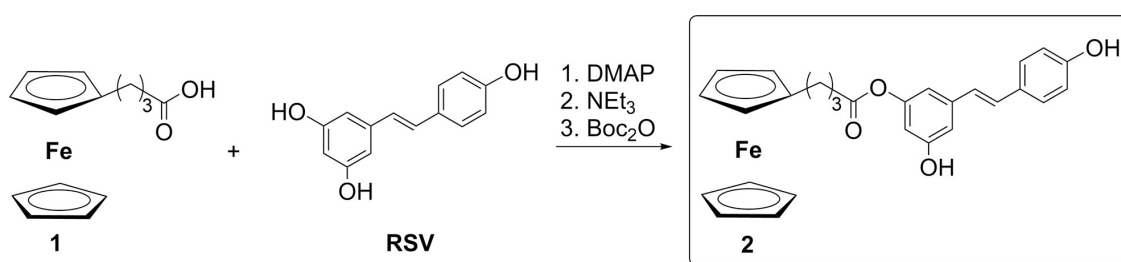


Figure 4. The chemical structures of (a) resveratrol (**RSV**) and (b) ferrocene-**RSV** analog **VI**.



Scheme 1. Synthesis of ferrocene-**RSV** conjugate **2**.

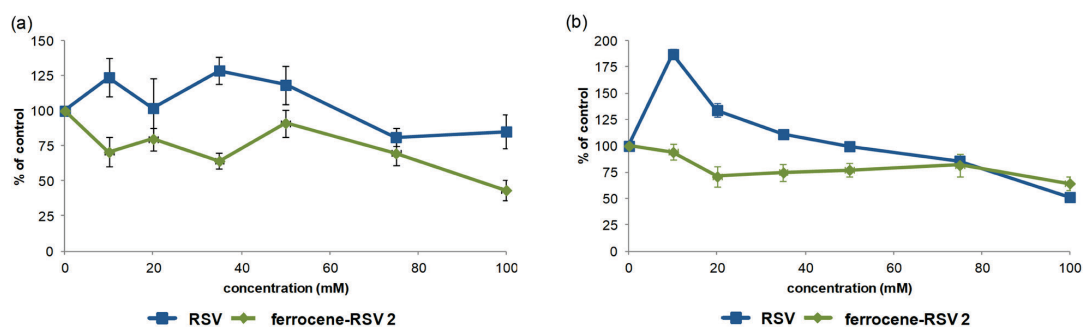


Figure 5. *In vitro* anti-proliferative effect of RSV and ferrocene-RSV conjugate **2** against (a) hepatoblastoma (HepG2) cells and (b) normal ovary cells (CHO-K1).

mannose and ferrocene in order to obtain a set of compounds that enables the more precise evaluation of the structural requirements for higher binding affinity of ferrocene-containing inhibitors of hemagglutination.

The condensation of the organometallic moieties with mannopyranoside acid was realized through ester and amide bonding, respectively (Scheme 2). The esterification of the mannopyranoside acid **7 α , β** with ferrocene alcohols **3** and **4** in the presence of stoichiometric amount of Boc_2O and catalytic amount of DMAP gave *O*-protected ester conjugates **8 α , β** and **9 α , β** . The synthetic pathway to obtain amide conjugates **12 α , β** and **13 α , β** started by Boc-deprotection of carbamates **5** and **6** in acidic milieu. The obtained hydrochloride salts were treated with an excess of NEt_3 to liberate free amines available for coupling with previously activated acid **7 α , β** to give *O*-protected amides **14 α , β** and **15 α , β** . Considering the α -anomeric preference of bacterial lectin FimH, the anomeric mixtures of the synthesized bioconjugates were separated by preparative thin layer chromatography and α -anomers of ferrocene conjugates with mannose were subjected to debenzoylation to give goal compounds **10 α** , **11 α** , **14 α** and **15 α** . The next step was to evaluate the minimal concentration of the synthesized bioconjugates required to prevent FimH-mediated agglutination of guinea-pig erythrocytes, that was expressed as inhibition titer (IT) and compared to those of a reference inhibitor, methyl α -D-mannoside (MeMan) to give relative IT (RIT). Although we have already observed that the elongation of the alkyl chain in compound **11c** was accompanied with the increment of the inhibitory activity,^[29] the herein obtained results revealed that the alkyl chain length is not of decisive importance for FimH-mediated binding of the investigated ferrocenes **10 α** , **11 α** , **14 α** and **15 α** . Since the compound **15 α** displayed 2-fold increment of inhibitory activity in comparison with herein studied compounds and 14-fold increment in comparison to standard MeMan (Figure 6), it is more likely that replacement of an ester linkage in **10 α** with amide linkage in **15 α** (both containing butyl spacer between ferrocene

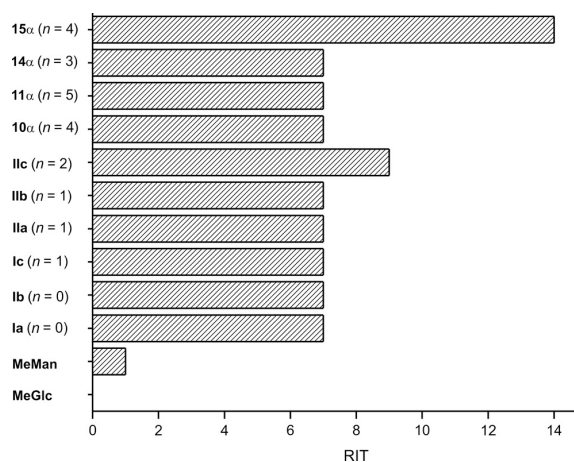


Figure 6. Inhibition of hemagglutination of guinea-pig erythrocytes by type 1 fimbriated *E. coli* HB101 (pPK14).

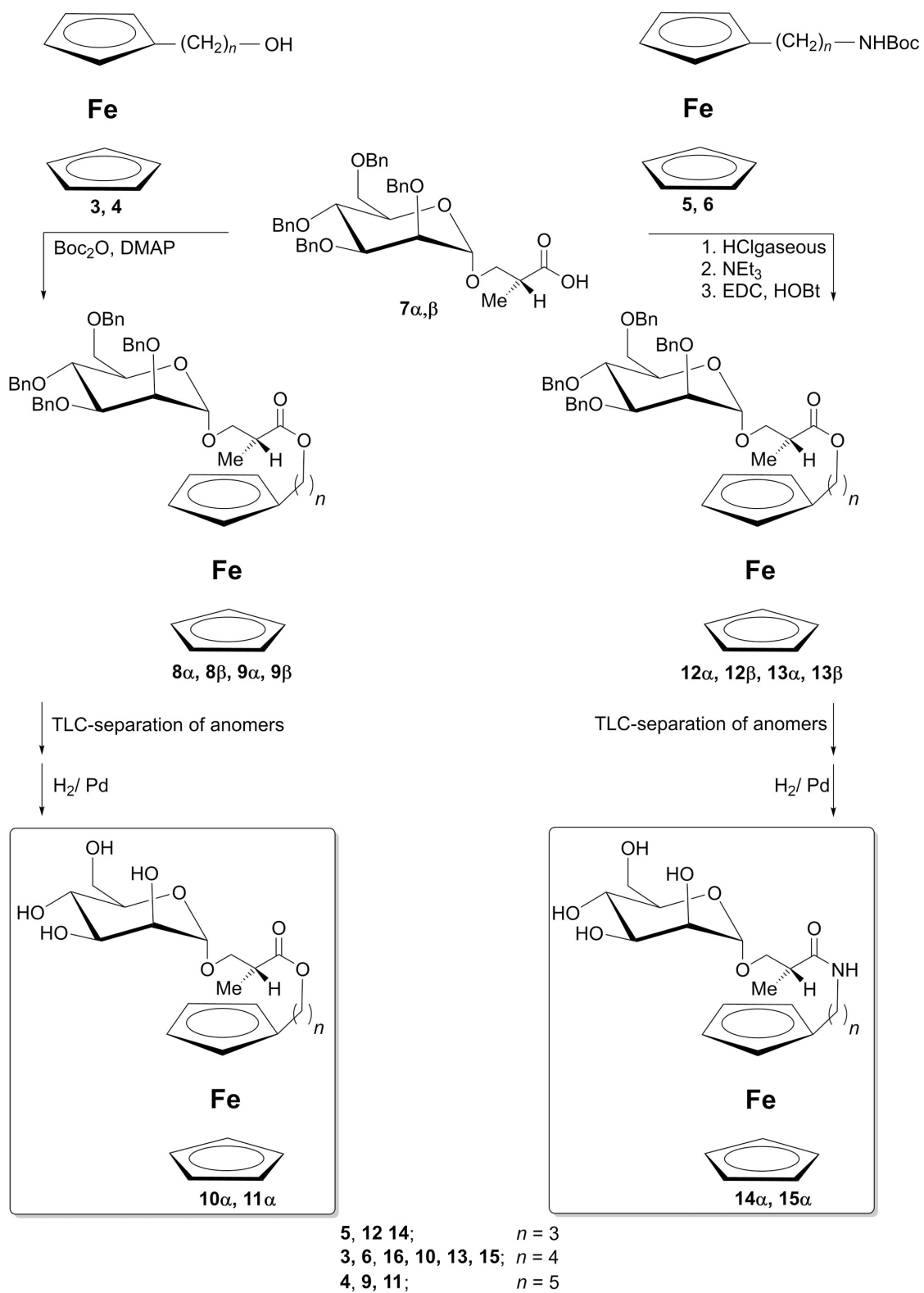
moiety and linkage) strongly influences the inhibitory potential.

Our ongoing research is directed to explore if the aromatic modification of the most potent FimH antagonist **15 α** will improve lipophilicity and binding affinity in the hydrophobic cavity of the mannose binding site of FimH, founded to be flanked with aromatic tyrosine residues.

II. CONFORMATIONAL PROPERTIES OF FERROCENE PEPTIDOMIMETICS

Oxalamide-bridged Ferrocene **17**

Peptides experience serious challenges (low metabolic stability towards proteolysis, the poor membrane permeability and the interactions with undesired receptors due to their conformational flexibility) on their way to become applicable for medicinal purposes. These obstacles can be overcome by using peptidomimetics.^[49,50] Among the numerous approaches in the design and synthesis of



Scheme 2. Synthesis of mannose-ferrocene conjugates 10, 11, 14 and 15.

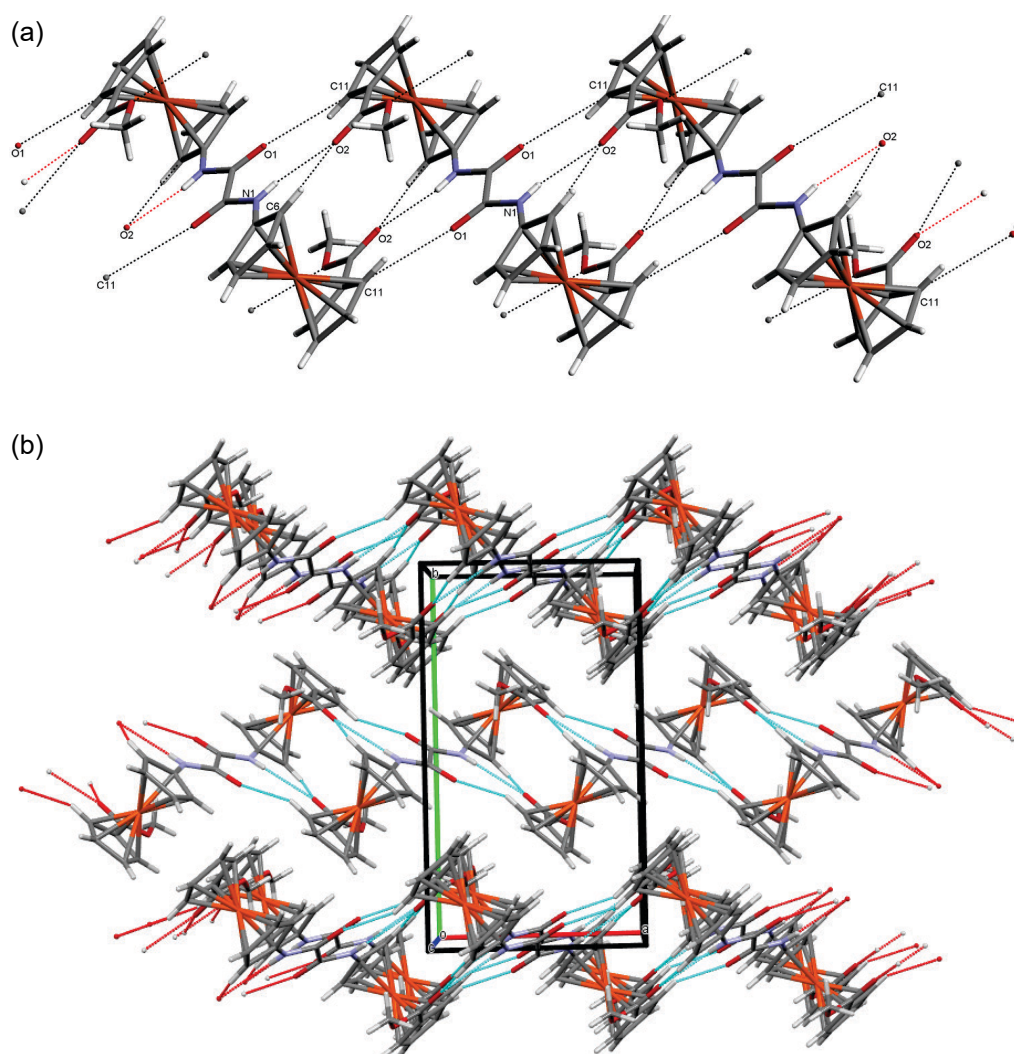


Figure 8. Crystal packing of oxalamide **17**. (a) Two C–H···O and one N–H···O hydrogen bonds connect the neighbouring molecules. (b) View along the *c* axis reveals that the crystal packing is realized by stacking of the hydrogen bonded staircase patterns.

In vitro screening of oxalamide **17** revealed proliferative as well as cytotoxic effect on normal human embryonic kidney cells (HEK293T) and tumour HepG2 cells (Figure 9). The observed dual effect of oxalamide **17** is attributed to the biological phenomenon named hormesis, that is characterised by a low dose stimulation or beneficial effect and high-dose inhibition or toxic effect.^[69–70] Biphasic dose-response effect had not been reported for ferrocenes yet. The cytotoxic *i.e.* antiproliferative activity of the oxalamide-bridged ferrocene **17** on the normal HEK293T cell line was weaker than in HeLa cancer cell line, whilst the displayed proliferative effect was most pronounced on normal HEK293T cells, and was not observed in tumour HeLa cells. These findings implicated the therapeutic potential of oxalamide-bridged ferrocene **17**, either as an anticancer agent, or as a stimulator of cell growth.

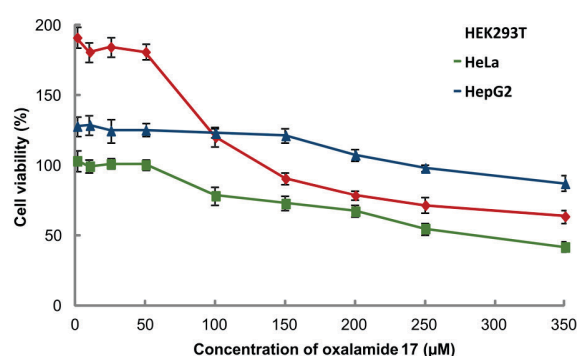


Figure 9. Effect of oxalamide-bridged ferrocene **17** on HEK293T, HeLa and HepG2 cell viability. The lines connecting the measured points are drawn to enhance clarity.

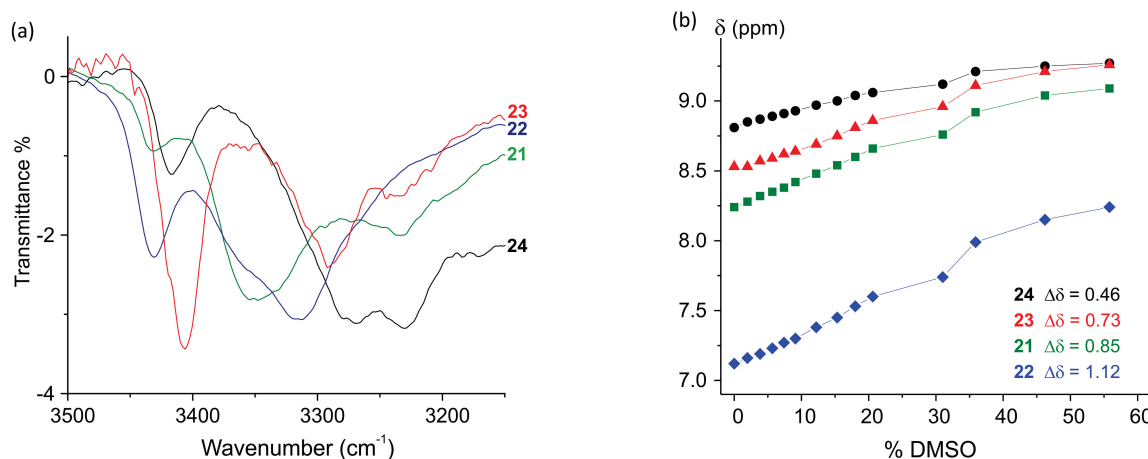


Figure 10. (a) The NH stretching vibrations in concentration-dependent IR spectra of **21–24** in CH₂Cl₂ ($c = 5 \times 10^{-2}$ M), (b) Solvent dependence of NH chemical shifts at varying concentrations of *d*₆-DMSO in CDCl₃ ($c = 2.5 \times 10^{-2}$ M, 298 K) to probe exposed vs. hydrogen-bonded amides.

Bioconjugates of 1'-Aminoferrocene-1-carboxylic Acid and Proline **21–24**

Besides its ability to induce turn structures when incorporated in peptides,^[71–73] proline undergoes *cis-trans* isomerization, a process that regulates numerous biological events such as cellular uptake, oligomerization, folding and catalysis. Therefore, in continuation of our work on ferrocene peptides **IV** we were interested to determine the impact of proline unit on conformational and biological properties of the bioorganometallics **21–24**.^[74]

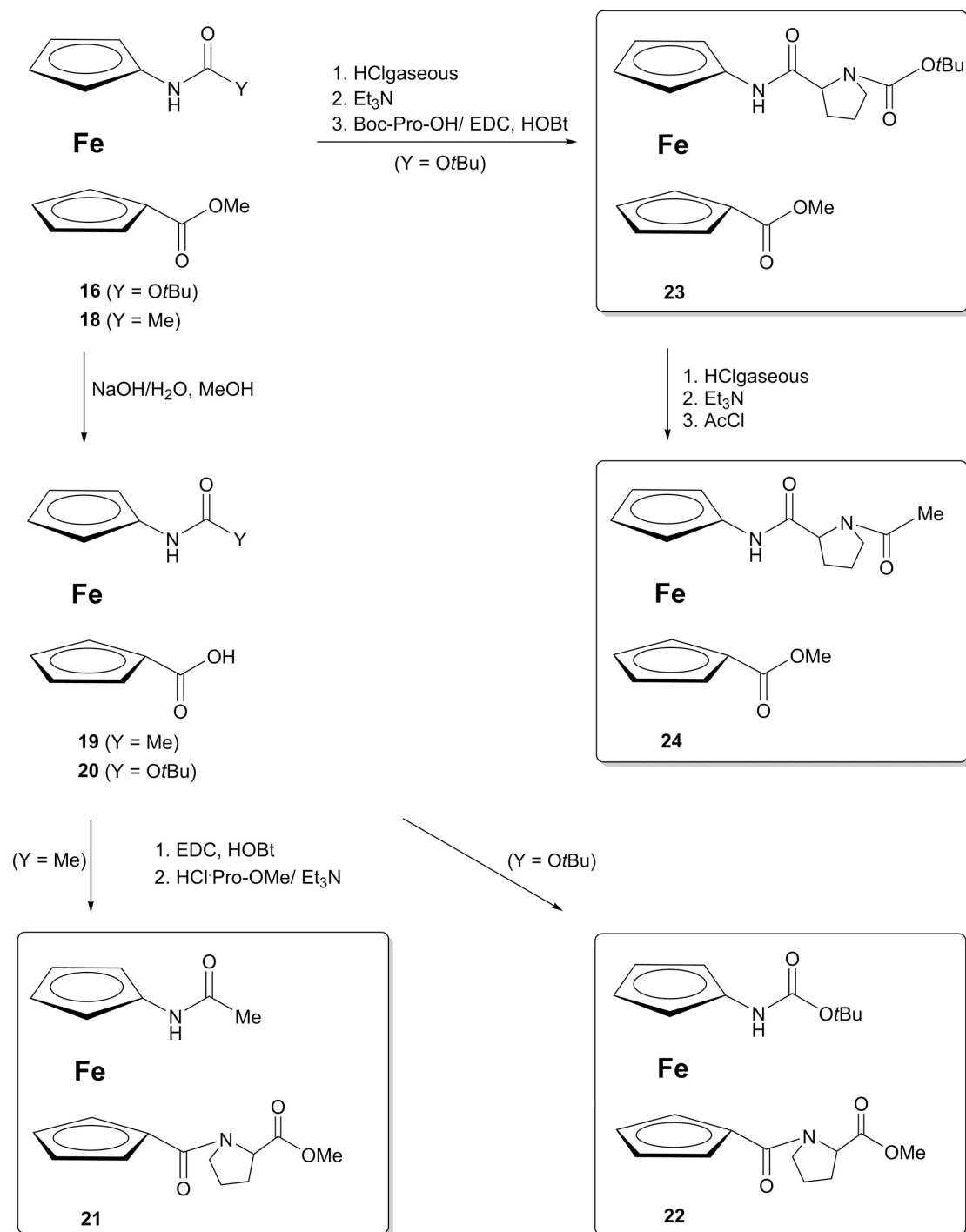
Ac–NH–Fn–CO–Pro–OMe (**21**) and Boc–NH–Fn–CO–Pro–OMe (**22**) were prepared by coupling of *N*-protected 1'-aminoferrocene-1-carboxylic acid (**19/20**) with *C*-protected proline following the above described coupling procedure. Boc–Pro–NH–Fn–COOMe (**23**) and Ac–Pro–NH–Fn–COOMe (**24**), with an exchanged sequence of constituent amino acid relative to **21** and **22**, were prepared from Boc–NH–Fn–COOMe (**16**). Upon Boc-deprotection and coupling with activated Boc–Pro–OH the goal compound **23** was obtained. Its Boc-group was transferred to Ac giving Ac–Pro–NH–Fn–COOMe (**24**) (Scheme 4).

Proline-containing bioconjugates **21–24** were subjected to standard spectroscopic methods (IR, NMR and CD spectroscopy) to explore their conformational behaviour. The amide stretching regions of the IR spectra indicated the presence of both associated (below 3400 cm⁻¹) and free states (above 3400 cm⁻¹). It is evident from the Figure 10a that (i) the population of hydrogen-bonded NH groups of peptides **21**, **22** and **24** is increased in comparison to peptide **23**, and (ii) the intensities of hydrogen-bonded NH absorption bands of analogues **21–24** in relation to their free NH band depended on the employed blocking group. Thereat, the reduced content of the associated NH bands was observed for peptides **22** and **23**, due to the steric

hindrance imparted by bulky Boc groups. To access whether the hydrogen-bonded NH groups were engaged in intra- or intermolecular manner, the concentration dependence of NH absorption bands was tested. The unchanged ratio of the associated and free NH bands upon successive dilution suggested the intramolecular employment of NH groups.

Hydrogen-bonding behaviour of bioconjugates **21–24**, predicted by IR data, was corroborated by the downfield shifts ($\delta > 7$ ppm) of their NH groups in non-polar CDCl₃. The almost preserved amide chemical shifts upon dilution from 50 mM to 6.25 mM or heating from 258 K to 328 K strongly support the intramolecular hydrogen bonding patterning, suggested by concentration-independent IR measurements. In order to evaluate the strength of IHBs, DMSO titration experiments were carried out (Figure 10b). The most downfield shifted NH_{Fca} of **24** exhibited the lowest sensitivity to DMSO and therefore was considered to be involved in a strong IHB. More pronounced changes of amide shifts in the presence of DMSO were observed for **21** and **23**, indicating their engagement in IHBs of medium strength. Since the most upfield shifted NH_{Fn} of **22** was found to be the most DMSO-sensitive, its participation in a weak IHB was suggested.

The NMR data obtained upon heating or DMSO titration revealed *cis/trans* isomerization of proline peptide bonds. The complete coalescence of the two peaks that correspond to *cis* and *trans* isomers occurred upon heating from 258 K to 328 K due to the medium (**23**) and rapid (**21**, **22** and **24**) isomerization. The abundance of *trans* amide in peptide **24** upon titration with DMSO corroborated the assumption of its involvement in strong IHB that induced the isomer locking, while the complete coalescence of amide resonances of peptide **22** was caused by engagement of NH group in weak IHB, as it was suggested by its pronounced upfield shifting in the presence of DMSO.

Scheme 4. Synthesis of bioconjugates **21–24**.

The IHB patterning of peptides **21–24**, proposed by IR and ¹H NMR data, was strongly supported by NOE spectroscopy. The interstrand NOE contacts NH_{F_n}→CH_{α_{Pro}} and NH_{F_n}→Me_{COOMe} accounts for NH_{F_n}···OC_{Pro} IHB in peptides **21** and **22**, while intrastrand NOE contacts of NH_{F_n} with *N*-

terminal protons of **23** and **24** point to NH_{F_n}···OC_{Pro} IHB (7-membered γ-turn) (Figure 11).

The previous work on ferrocene-containing peptides revealed that the insertion of ferrocene chromophore (λ ~ 480 nm) into the chiral peptide environment enables

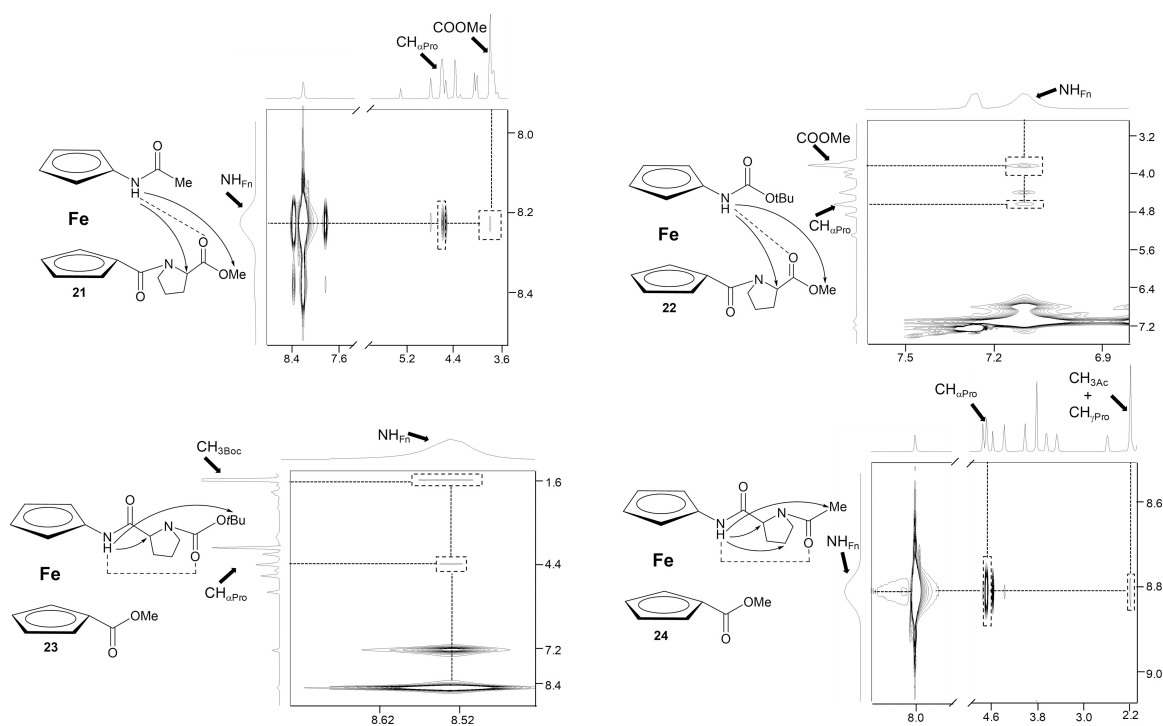


Figure 11. The interchain NOE connectivities between the C- and N-termini of **21** and **22** and the intrachain NOE connectivities of **23** and **24** (the proposed IHBs are depicted with dashed lines).

hydrogen bonding between podand peptide chains. Conformational changes, promoted by insertion of organometallic template into peptide chain, lead to the adoption of ordered structures that induce Cotton effect in ferrocene region.

The absolute values of Cotton effects of **21-24**, ranged between 500 and 1000 $\text{deg cm}^2 \text{dmol}^{-1}$ corresponded to those observed for their alanine analogues,^[33b] indicating the presence of an ordered structures in CH_2Cl_2 (Figure 12). To address the assumption that peptide **22** was involved in the weakest IHB in

comparison to peptides **21**, **23** and **24**, their CD activity in the presence of DMSO was tested. As expected, the absence of Cotton effect was observed for peptide **22**, due to the cleavage of weak IHB and loss of chiral organization.

The intrastrand hydrogen bond in peptide **23**, predicted by NMR study, persisted in the solid state as well. Its conformation was stabilised by one N-H...O and four weak C-H...O intramolecular hydrogen bonds (Figure 13a). An additional stabilization was achieved through interchain dipolar interaction between CO_{Fn} and NH_{Fn} (Figure 13b).

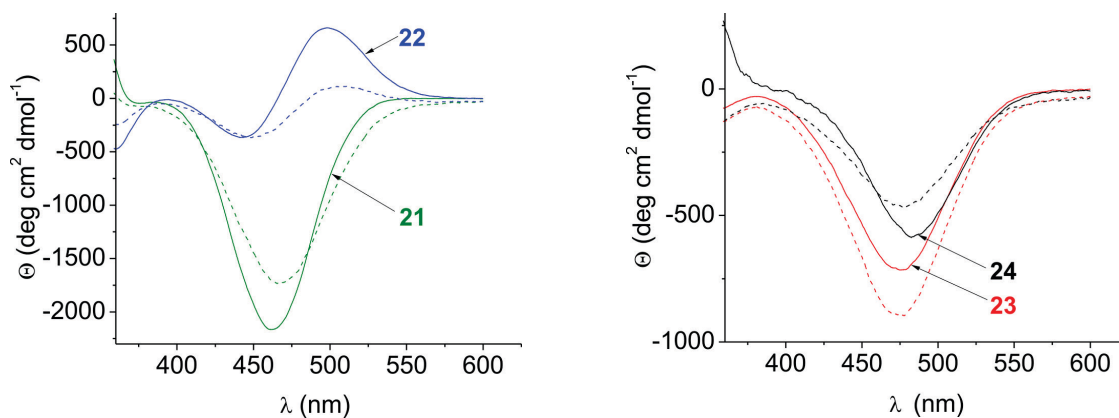


Figure 12. Cotton effects in chirality-organized ferrocene peptides **21-24** in CH_2Cl_2 [(—) $c = 1 \times 10^{-3} \text{ M}$] and CH_2Cl_2 ($c = 1 \times 10^{-3} \text{ M}$) containing 20% of DMSO (---).

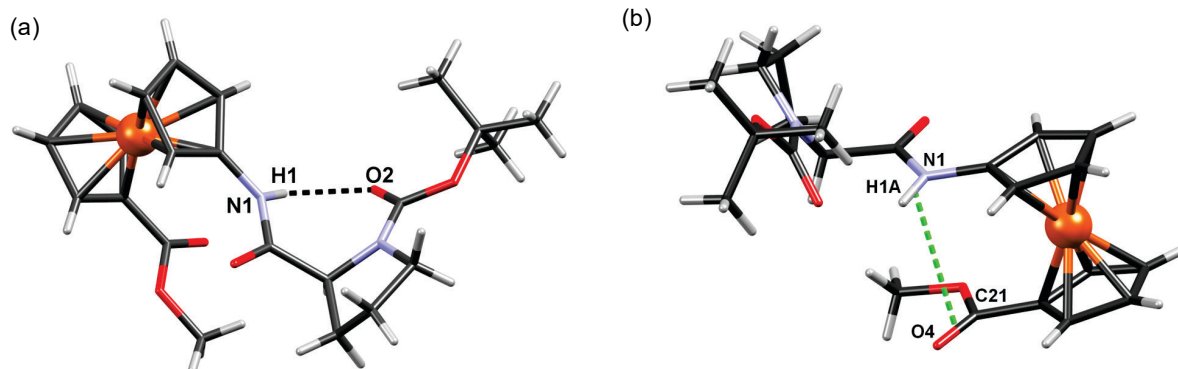


Figure 13. (a) Conformation of Boc-Pro-NH-Fn-COOMe (**23**) in the crystal stabilised by intrachain 7-membered IHB-ring (γ -turn), (b) an additional stabilization of Boc-Pro-NH-Fn-COOMe (**23**) through interchain intramolecular dipolar interaction.

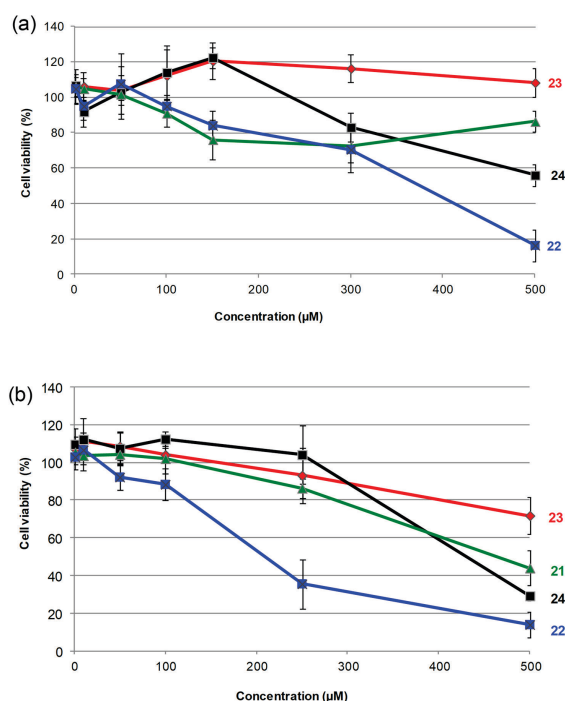


Figure 14. Effects of peptides **21–24** on (a) MCF7 and (b) HeLa cells viability. The lines connecting the measured points are drawn to enhance clarity.

The anticancer potential of peptides **21–24** was tested *in vitro* and evaluated on the basis of their ability to inhibit growth of MCF7 and HeLa carcinoma cells. While the 50 % inhibition of cell growth was not detected by the compounds **21**, **23** and **24**, the peptide **22** exhibited the highest cytotoxicity in MCF7 and HeLa cells (Figure 14). Taking into account the lipophilicity as an important requirement in drug design, the obtained results might be attributed to the increased lipophilicity of peptide **22** ($R_f = 0.50$) in comparison to more polar analogues **21** ($R_f = 0.30$), **23** ($R_f = 0.33$) and **24** ($R_f = 0.22$).

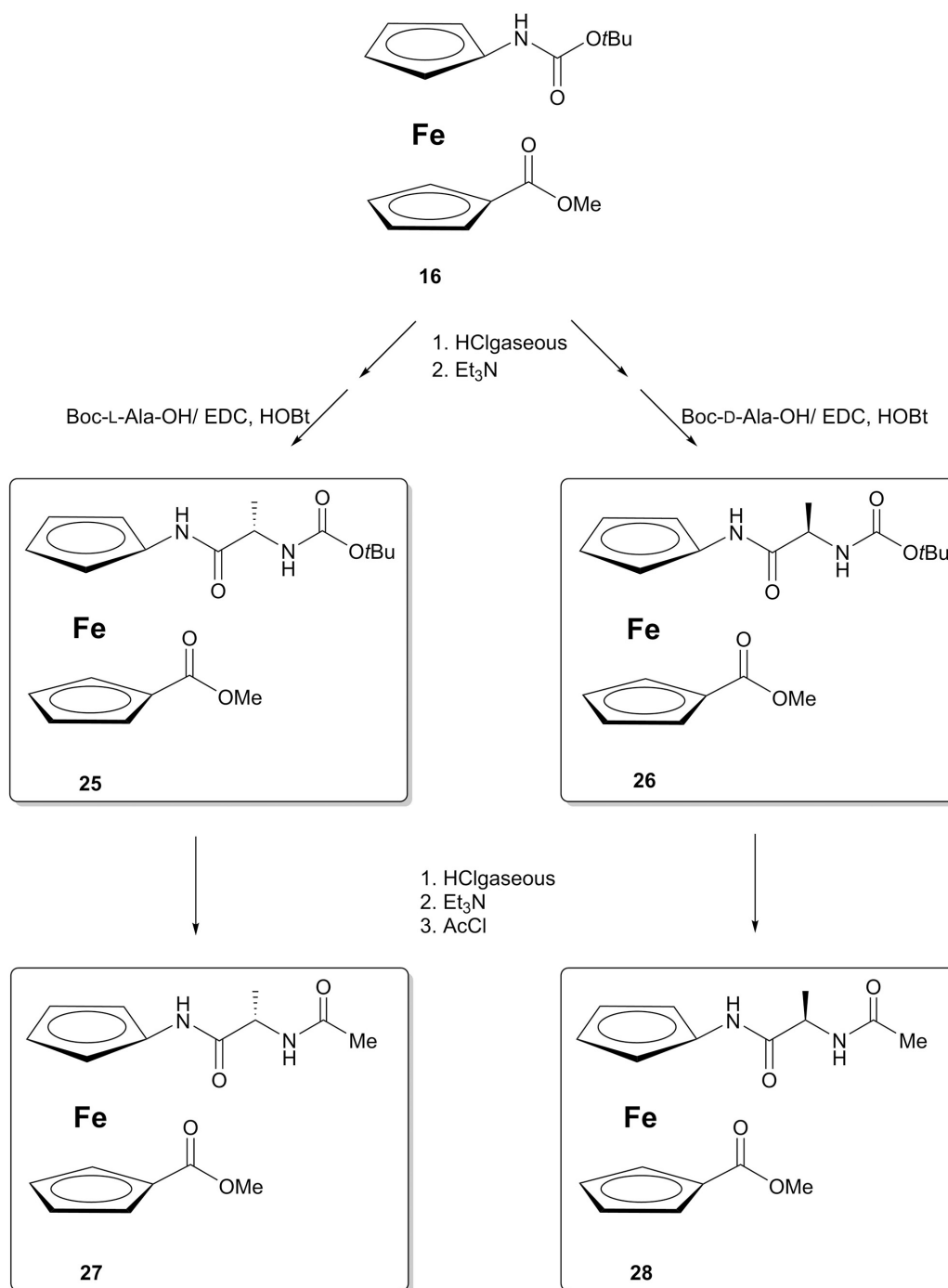
Bioconjugates of 1'-Aminoferrocene-1-carboxylic Acid and Alanine **25–28**

The synthesis of bioconjugates **25–28**^[75] (Scheme 5) has been performed by using the synthetic protocol described above for the preparation of proline-containing ferrocenes, with aim to obtain the simplest models to study the influence of the backbone chirality and terminal group bulkiness on conformational properties of ferrocene-containing peptides.

The synthesized bioconjugates were subjected to detailed conformational analysis (IR and NMR spectroscopy and DFT study) in order to explore if the replacement of the bulky Boc group with Ac function and L- to D-Ala exchange affects their conformational behaviour.

The ratios of free and associated NH bands in IR spectra of the examined compounds indicated the increased fraction of hydrogen bonded NH groups in Ac-peptides **27** and **28**, most likely owing to steric hindrance of Boc groups in **25** and **26**. Results from the dilution experiments revealed the weakening of the both signals corresponding to free ($\sim 3424\text{ cm}^{-1}$) and bonded ($\sim 3300\text{ cm}^{-1}$) NH groups and appearance of a single band slightly shifted to $\sim 3400\text{ cm}^{-1}$ (Figure 15a), thus disabling reliable determination of the character of association.

The resonances of NH_{Fn} groups of peptides **25–28** and NH_{Ala} groups of Ac-peptides **27** and **28** were observed at downfield region and were therefore expected to be involved in HB. The upfield shifted NH_{Ala} groups of Boc-peptides **25** and **26** corroborates the assumption that hydrogen bonding was somewhat difficult in the presence of Boc group. To elucidate the possible intramolecular nature of hydrogen bonds, concentration- and temperature-dependent NMR spectra were measured, without expecting any discernible changes in chemical shifts of amide protons engaged in IHBs. The observed negligible dependence of the chemical shifts on concentration and temperature (Figure 15b) strongly



Scheme 5. Synthesis of bioconjugates **25–28**.

supported the intramolecular hydrogen bonding behavior. Furthermore, an increased temperature dependencies of concentration-independent NH_{Fn} [**25** (–5.6 ppb/K), **26** (–6.0 ppb/K), **27** (–9.6 ppb/K), **28** (–9.6 ppb/K)] and NH_{Ala} [**27** (–6.4 ppb/K), **28** (–7.2 ppb/K)] reflected initially shielded states transferred to unshielded environment by unfolding of conformations organized through IHBs.

Evaluation of hydrogen bond strength was carried out by DMSO titration. Rapid rise in the slope of the titration curves in the region below 20 % DMSO was caused by significant changes in chemical shifts ($\Delta\delta > 1$ ppm) over the range of the ¹H NMR experiment, owing to participation of NH groups in weak IHBs (Figure 15c).

The position of hydrogen bond donating and

accepting groups in peptides **25–28** allowed the formation of both inter- and intrastrand IHBs. The interstrand contacts between C- and N-termini required for turn formation^[76] were observed in NOESY spectra of the examined compounds [*t*Bu_{Boc}→Me_{COOMe} (**25/26**) and Me_{Ac}→Me_{COOMe} (**27/28**)] and might account for NH_{Ala}⋯OC_{COOMe} IHB. Regarding the intrastrand IHBs, the NOE contacts NH_{F_n}→Me_{Ac} in spectra of Ac-peptides **27** and

28 were detected, while the contacts of NH_{F_n} and protons of *tert*-butyl group in **25** and **26** were not observed, due to the absence of hydrogen bonding along the corresponding strand. Besides that, the larger frequency of NOE contacts for NH_{F_n} in Ac-peptides **27** and **28** in comparison to those of NH_{F_n} in Boc-peptides **25** and **26** additionally supported the assumption of steric hindrance imposed by *tert*-butyl group (Figure 16).

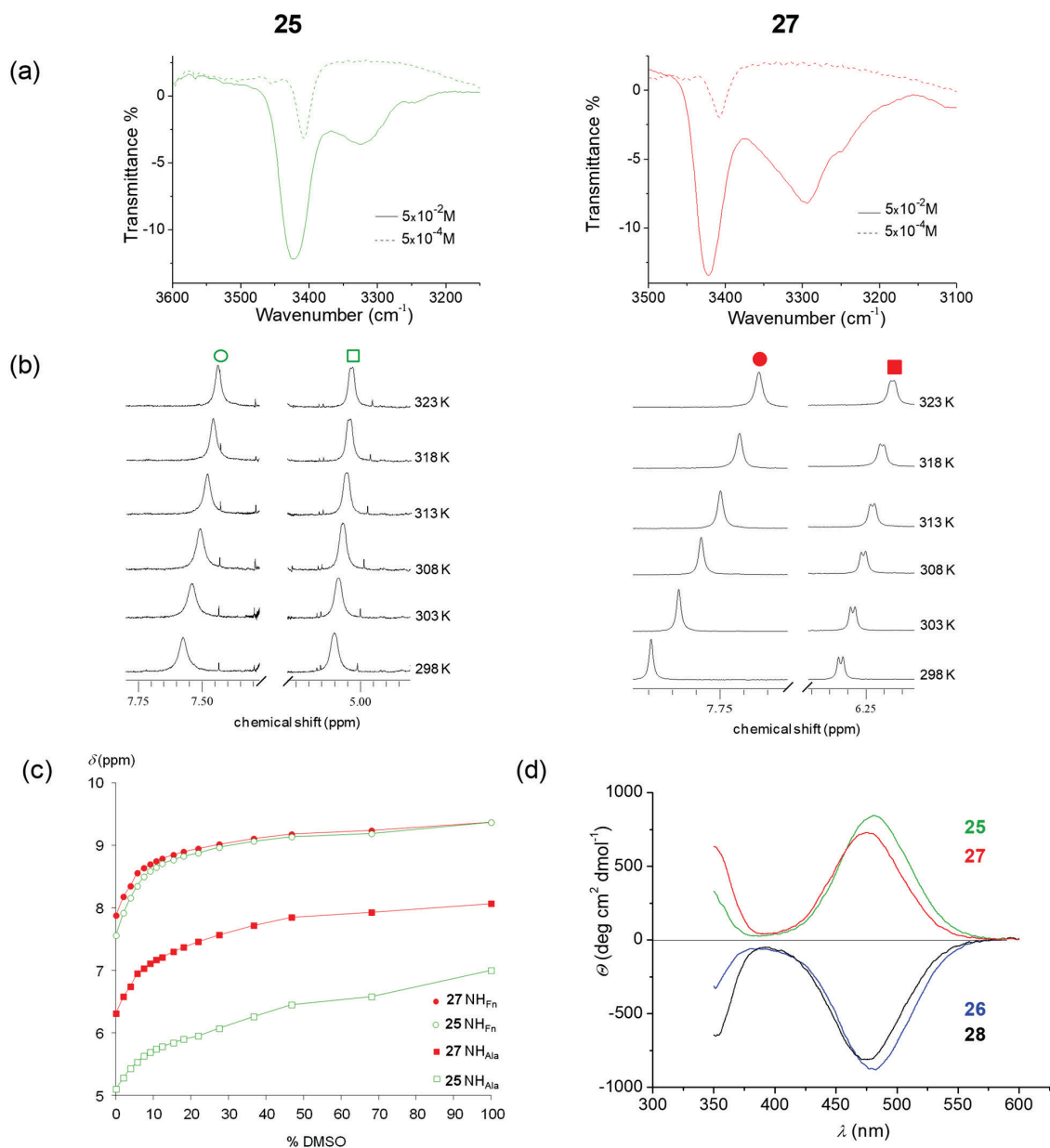


Figure 15. (a) The NH stretching vibrations in concentration-dependent IR spectra of **25** and **27** in CH₂Cl₂, (b) Temperature dependence of NH chemical shifts ($c = 2.5 \times 10^{-2}$ M) in the temperature range of 298–328 K, (c) Solvent dependence of NH chemical shifts at varying concentrations of *d*₆-DMSO in CDCl₃ ($c = 2.5 \times 10^{-2}$ M, 298 K) to probe exposed vs. hydrogen-bonded amides, (d) Cotton effects in chirality-organized ferrocene peptides **25–28** in CH₂Cl₂ ($c = 1 \times 10^{-3}$ M). The compatible results on IR and temperature-dependent NMR measurements were obtained for enantiomeric pairs **26** and **28**.

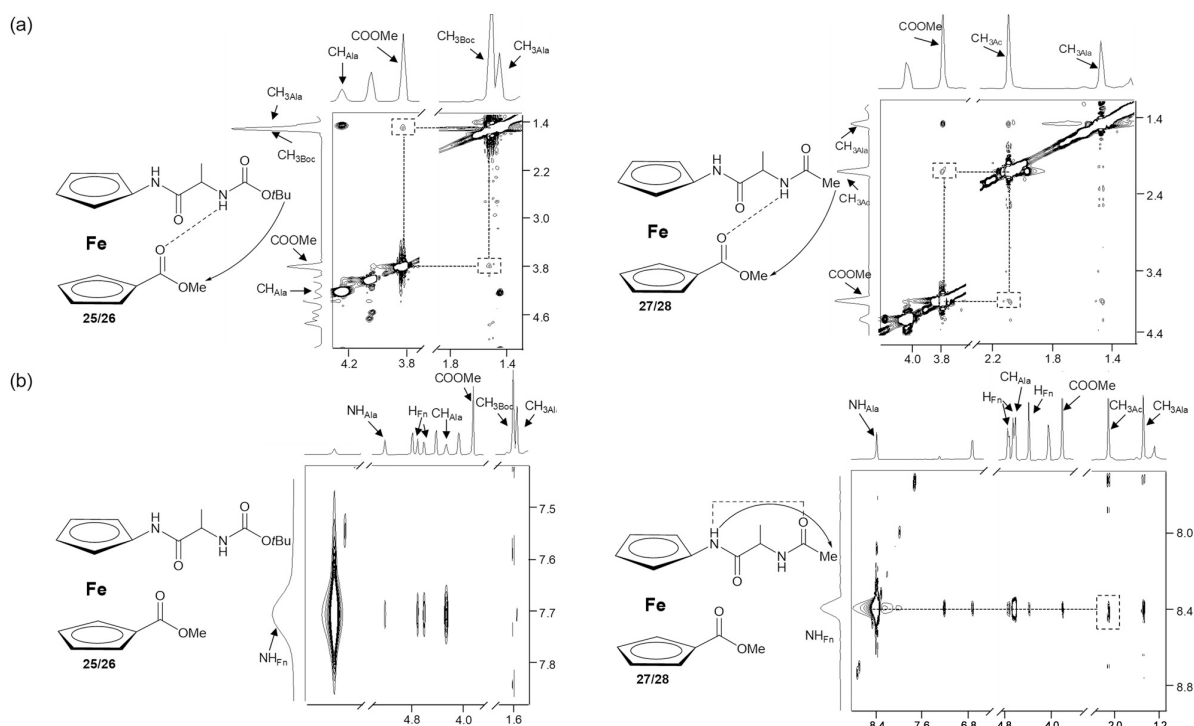


Figure 16. (a) The interchain NOE connectivities between C- and N-termini of **25–28** and (b) intrachain NOE contacts for NH_{Fn} in Boc-peptides **25/26** and Ac-peptides **27/28** (the proposed IHBs are depicted with dashed lines).

These assumptions about IHB patterning were confirmed with CD signals in the region of ferrocene chromophore (Figure 15d). Mirror image arrangement of the CD curves of **25** and **26** as well as **27** and **28** resulted from their conformational enantiomeric relationship. Due to our previous findings,^[33] the positive Cotton effects of (*R*)-**25** and (*R*)-**27** were attributed to the helices of (*P*)-orientation, while corresponding enantiomers (*S*)-**26** and (*S*)-**28** adopted an opposite (*M*)-oriented helices.

In our research on ferrocene-containing peptides, an experimental data were usually augmented with molecular modeling studies to obtain a detailed picture regarding hydrogen bonding. The complete conformational analysis of Boc-peptide **25** and Ac-peptide **27** was performed using combination of molecular mechanics and DFT calculations. Relative distribution of conformers for peptides **25/27** with L-Ala moieties was the same for their enantiomers **26/28** with D-Ala. The pseudo-torsion angle defining helicity was opposite in pair of enantiomers (for example, one enantiomer has (*P*)-1,2' and the other (*M*)-1,5' configuration), while the hydrogen bonding pattern was the same, as the molecular geometry of one enantiomer is only the mirror image of the other.

The DFT analysis results that predicted three IHB motifs **A–C** were compatible with NMR data (Figure 17). The most stable conformers of **25** and **27** were found to adopt

$\text{NH}_{\text{Fn}}\cdots\text{OC}_{\text{Boc/Ac}}$ intrastrand IHB forming 7-membered ring [(γ -turn), (type **A**)] or $\text{NH}_{\text{Fn}}\cdots\text{N}_{\text{Ala}}$ intrastrand IHB forming 5-membered ring of the type **B**. In the ensemble of the most stable conformers, single interstrand $\text{NH}_{\text{Ala}}\cdots\text{OC}_{\text{Fn}}$ IHB of the type **C** was observed only in Ac-peptide **27**. The same observations were valid for their enantiomers **26** and **28**.

Bioconjugates of 1-Acetyl-1'-aminoferrocene with Amino Acids (**33–35**, **39–41**) and Their Monosubstituted Analogues (**30–32**, **36–38**)

Bioconjugates **33–35** (Boc-AA-NH-Fn-COMe ; AA = Gly, L-Ala, L-Val)^[77] and **39–41** [$\text{Boc}-(\text{AA})_2\text{-NH-Fn-COMe}$; AA = Gly, L-Ala, L-Val]^[78], derived by N-terminal elongation of Boc-NH-Fn-COMe , can also be considered as nonsymmetric analogues of ferrocene-containing peptidomimetics **IV** (Scheme 6). These derivatives were subjected to detailed CD, IR and NMR spectroscopic analysis, combined with theoretical investigation (DFT), to describe their preferred conformations in solution. Furthermore, to gain better insight on the hydrogen bond patterns in **33–35** and **39–41**, a complete set of their monosubstituted analogues **30–32** (Boc-AA-NH-Fn ; AA = Gly, L-Ala, L-Val) and **36–38** [$\text{Boc}-(\text{AA})_2\text{-NH-Fn}$; AA = Gly, L-Ala, L-Val] was synthesised and subjected to conformational analysis as well.

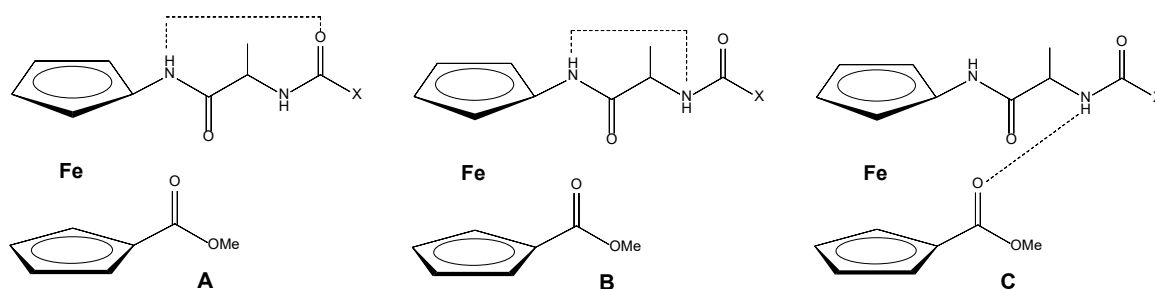
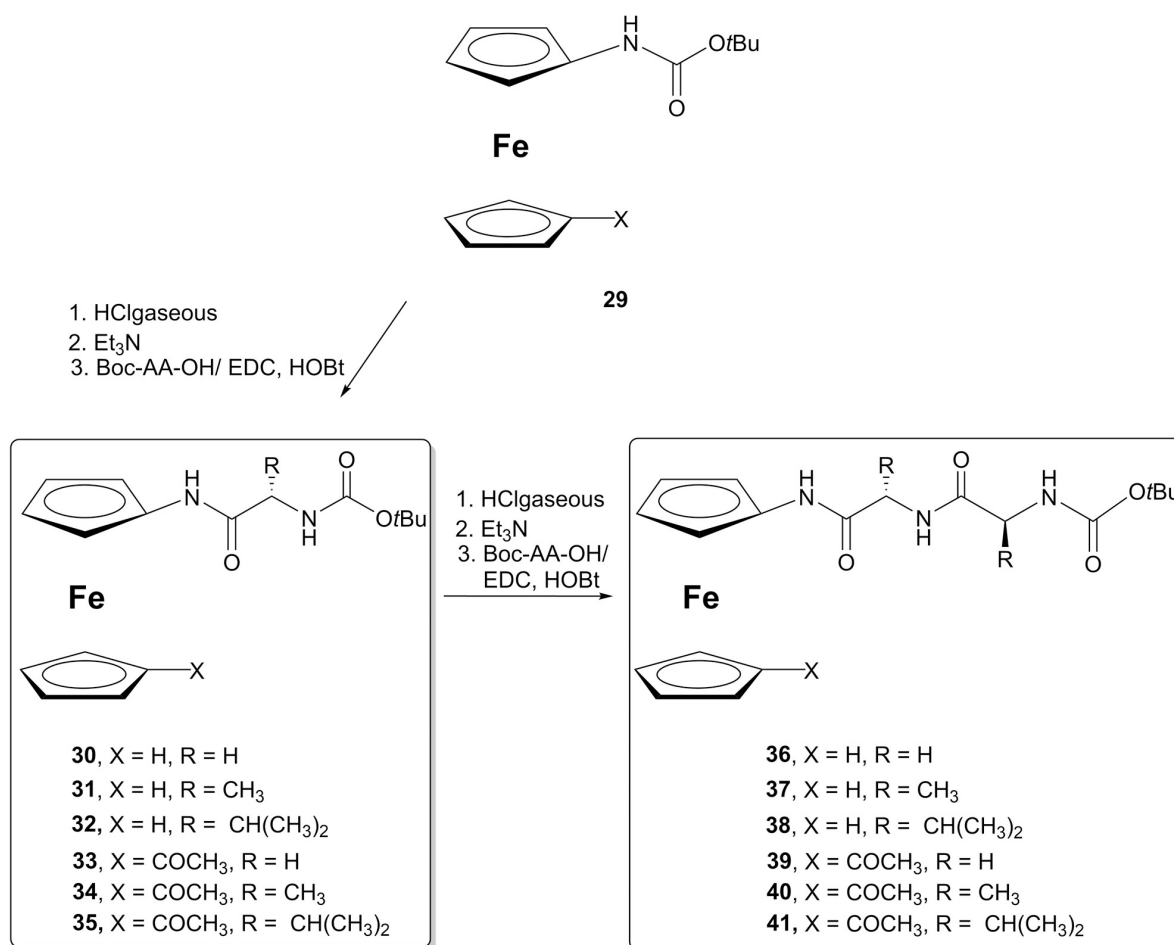


Figure 17. The intramolecular hydrogen bonding patterns observed in the ensemble of the most stable conformers based on computational study for **25** ($X = OtBu$) and **27** ($X = Me$).



Scheme 6. Synthesis of bioconjugates **30**–**41**.

The downfield resonance of NH_{Fn} (~7.7 ppm), observed in the NMR spectra of **30**–**35**, indicated its participation in a hydrogen bond. Although the NH_{AA} resonances were registered at high field (5.1–5.5 ppm), we did not exclude the possibility of involvement of these groups in hydrogen bonding due to examples of urethane NH groups resonating at high field in $CDCl_3$.^[79,80] During NMR dilution experiments in the concentration range of

1.5–100 mM any significant variation of NH_{Fn} resonances was not observed ($\Delta\delta < 0.2$ ppm), so we attributed the initial chemical shift to intramolecular hydrogen bonding. Furthermore, to determine the strength of bonds involving NH group directly attached to ferrocene, we performed DMSO titration experiments. As can be seen in Figure 18, the gradual addition of DMSO (from 0 to 30 % in $CDCl_3$) caused the dramatic downfield shift of NH_{Fn} protons of **32**

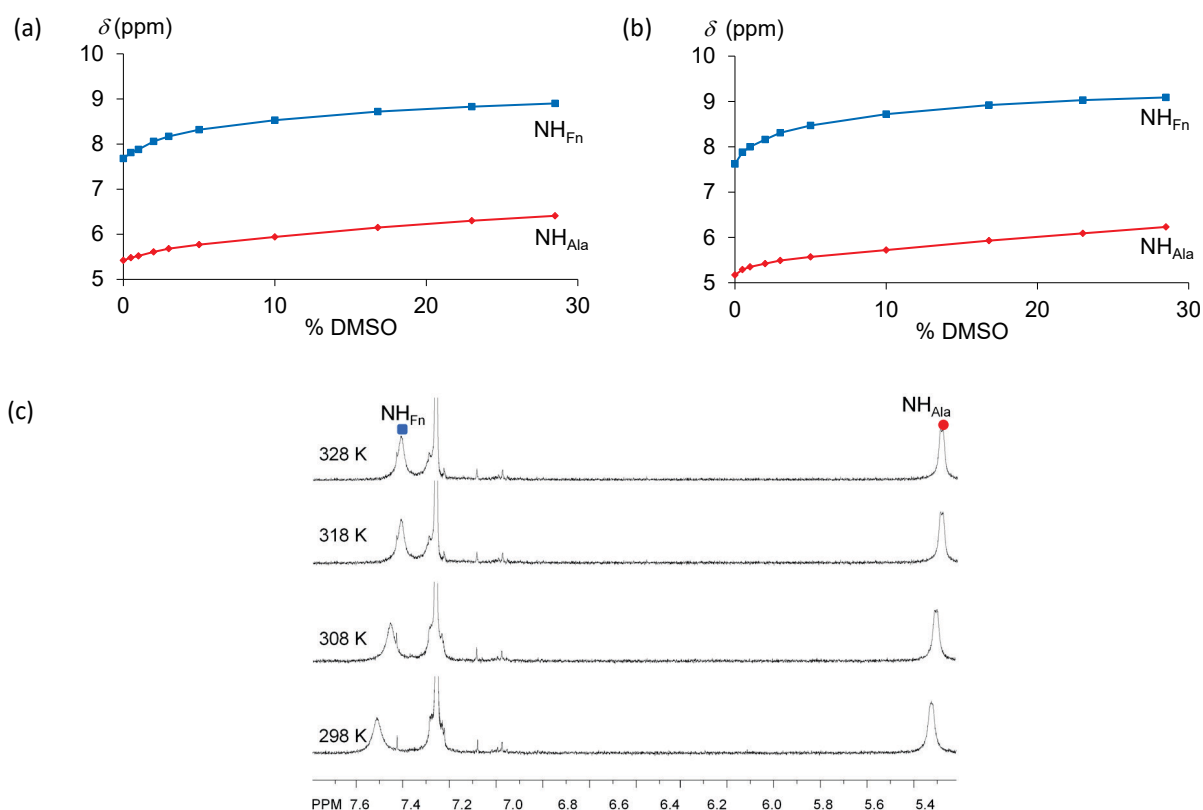


Figure 18. Solvent dependence of NH chemical shifts of compounds (a) **32** and (b) **34** at varying concentrations of *d*₆-DMSO in CDCl₃ ($c = 2.5 \times 10^{-2}$ M, 298 K) to probe exposed vs. hydrogen-bonded amides, (c) Temperature dependence of NH_{Fn} and NH_{Ala} chemical shifts of compound **34** ($c = 2.5 \times 10^{-2}$ M) in the temperature range of 298–328 K.

(1.22 ppm) and **34** (1.41 ppm), suggesting that these bonds are easily disrupted by the presence of competitive solvent. Similar solvent accessibility was observed for NH_{AA} group.

Furthermore, large temperature coefficients of NH_{Fn} protons in disubstituted conjugates ($\Delta\delta/\Delta T = -4.67$, -4.67 , and -6 ppb K⁻¹ for **33**, **34**, and **35**, respectively) were indication of an initially shielded NH groups which become exposed with increasing of temperature (Figure 18c).

The hydrogen-bond patterns found in the most stable conformers of **30–35**, derived from the computational study, are shown in Figure 19. The results of DFT study were in accordance with those derived from NMR measurements; in minimal energy conformer of all derivatives, NH group directly attached to the ferrocene was involved in a hydrogen bond with urethane carbonyl. Disubstituted conjugates (**33–35**) were additionally stabilized by an interchain bond between NH_{AA} and the acetyl carbonyl.

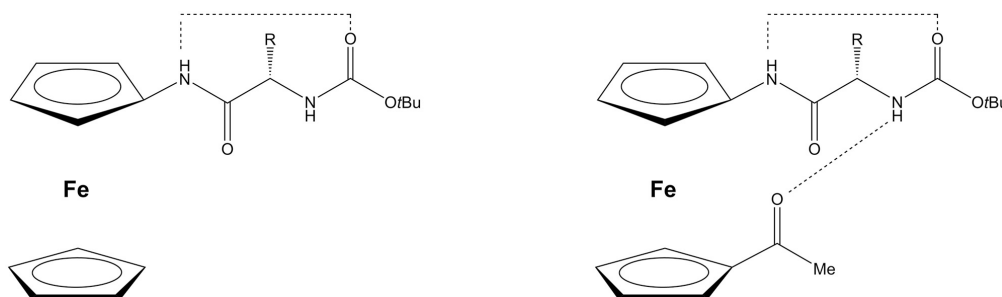


Figure 19. The intramolecular hydrogen bonding patterns observed in the most stable conformer based on computational study for mono- (**30–32**, left) and disubstituted conjugates (**33–35**, right).

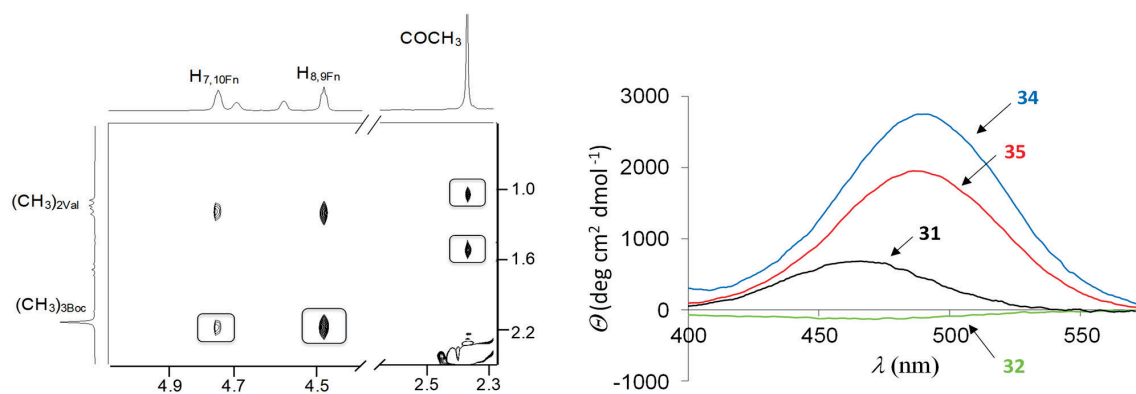


Figure 20. Important NOE interactions of **35** (left) and Cotton effects in chirality-organized ferrocene peptides **31**, **32**, **34** and **35** (right).

NOESY experiments and CD spectroscopy provided further evidence for interchain interactions in the disubstituted conjugates **33–35**. “Superimposable” orientation of substituents on cyclopentadienyl rings, caused by interstrand bonding, was supported by observation of NOESY cross-peaks shown on Figure 20 for derivative **35**. The visible regions of CD-spectra of chiral derivatives (**31**, **32**, **34** and **35**) are shown in the same Figure. Monosubstituted conjugates **31** and **32** exhibited a weak signal near UV/Vis absorption maximum of the ferrocene chromophore ($M_{\theta} = 683$ and -133 deg cm² dmol⁻¹), as expected for derivatives unable to form interchain hydrogen bonds.^[81] Medium-intensity CD-signals, observed in the spectra of **34** and **35** ($M_{\theta} = 2751$ and 1953 deg cm² dmol⁻¹), indicated an ordered chiral environment in the vicinity of ferrocene moiety arising from interstrand hydrogen bonding. The sign of Cotton effect founded in CD spectra of **34** and **35** was in accordance with previously described literature examples where bioorganometallics derived from L-amino acids exhibited positive CD signals, induced by *P*-helicity of energetically accessible conformers^[33b,74,75]

Peptides **36–41** were synthesised by *N*-terminal elongation of their lower homologues **30–35** and subjected to conformational analysis using IR and NMR spectroscopic techniques in combination with DFT calculations. In the solution IR spectra of all compounds signals belonging to hydrogen-bonded NH groups together with signals above 3440 cm⁻¹ due to presence of free NH groups were observed. We ruled out the possibility of intermolecular hydrogen bonding by performing IR-dilution experiment, over a concentration range of 50 to 0.5 mM (Figure 21a). Next, we undertook NMR study to find out which NH groups participate in hydrogen bonds as suggested by IR-spectroscopy. Involvement of NH attached to the ferrocene moiety in a hydrogen bond was indicated by its downfield shifted signal (~ 8.1 ppm) in spectra of all conjugates. In

contrast, signals of NH_{AA1} as well as the NH_{AA2} were registered at ~ 6.8 and ~ 5.2 ppm, indicating that former NH group equilibrates between bonded and non-bonded states and later does not participate in hydrogen bonds. Furthermore, in all conjugates NH_{Fn} and NH_{AA1} were significantly less accessible to the solvent than NH_{AA2} as can be seen from DMSO titration experiments, shown on Figure 21b.

In order to determine the dominant conformations of **36–41** in solution, search of the conformational space at the B3LYP/6-311 (+G(d,p) and LanL2DZ for iron) level of theory was performed. According to computational analysis, the lowest energy conformer of monosubstituted derivatives **36–38** was stabilized by β -turn-like structure *i. e.*, 10-membered hydrogen-bonded ring formed between the NH group closest to the ferrocene unit and the urethane carbonyl group (Figure 22). This finding was in agreement with the results obtained from NOE experiments. As can be seen in Figure 22, sequential dNN (*i, i + 1*) and d_NN (*i, i + 1*) connectivities, characteristic for β -turn, were observed in the NOESY spectra of conjugates **36–38**.

Furthermore, an ordered environment in the vicinity of ferrocene chromophore gave rise to a strong signal in CD spectra of chiral derivatives **37** and **38** (Figure 23). These results were in contrast with previous examples in which strong Cotton effects originate from helically chiral arrangements of the ferrocene moiety supported by interchain hydrogen bonds between the two podand peptide chains.^[33b] So, for the first time we demonstrated that a transfer of chiral information from a folded peptide chain to ferrocene chromophore can also give rise to a strong signals around the UV/Vis absorption maximum of the ferrocene chromophore ($\lambda_{\max} \approx 455$ nm).

In the analogous 1-acetyl derivatives (**39–41**), β -turn-like structures were destabilized according to computational study, NOESY and CD experiments. This findings can be explained by the fact that heteroannular introduction of

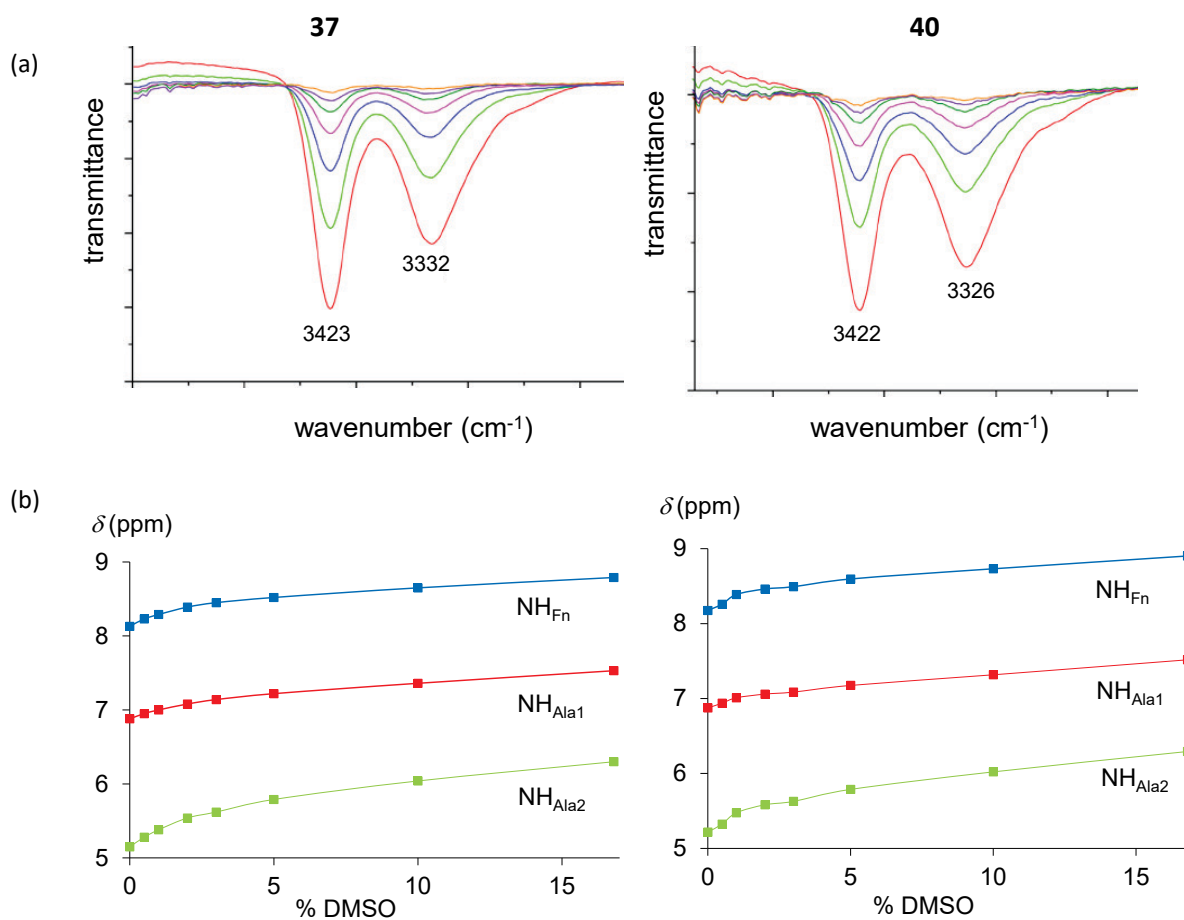


Figure 21. (a) The NH stretching vibrations in concentration-dependent IR spectra of **37** and **40** in CH_2Cl_2 ($c = 5 \times 10^{-2}$ M), (b) Solvent dependence of NH chemical shifts of compounds **37** and **40** at varying concentrations of d_6 -DMSO in CDCl_3 ($c = 2.5 \times 10^{-2}$ M, 298 K) to probe exposed vs. hydrogen-bonded amides.

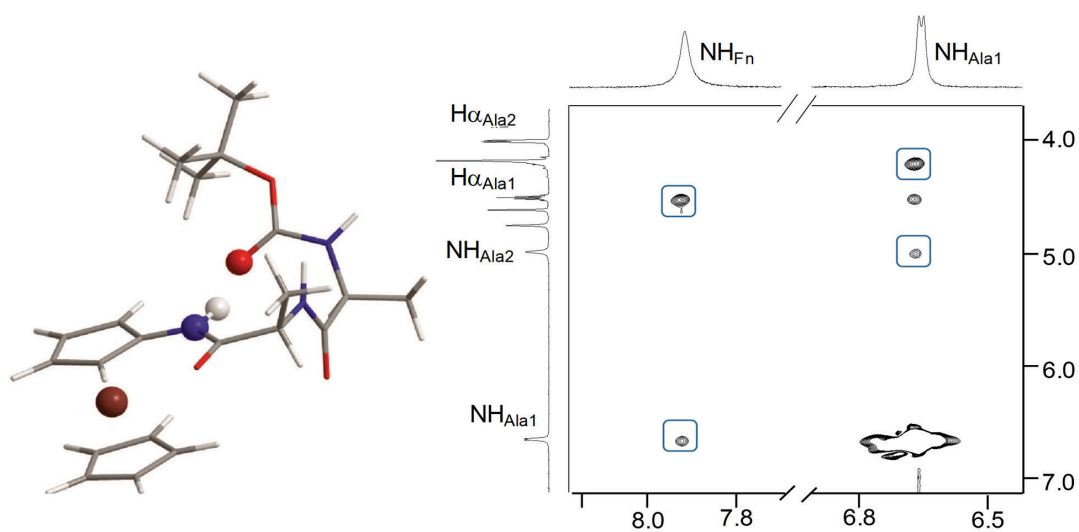


Figure 22. The most stable conformer and important interactions in NOESY spectrum of **37**.

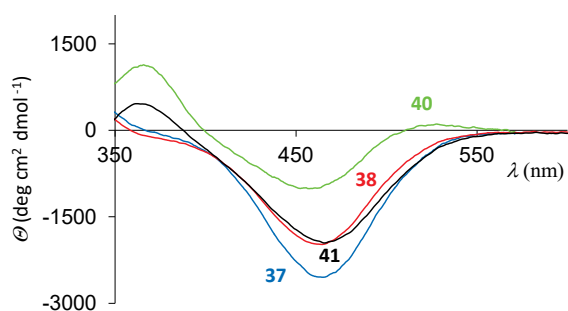


Figure 23. Cotton effects in chirality-organized ferrocene peptides **37**, **38**, **40** and **41** in CH_2Cl_2 ($c = 1 \times 10^{-3}$ M).

an additional hydrogen bond acceptor group (COMe) enabled the conjugates **39–41** to form interchain hydrogen bonds and to expand their accessible conformational space. The hydrogen bond patterns found in the ensemble of the most stable conformers based on computational study of derivatives **39–41** are shown in Figure 24.

Bioconjugates of Aminoferrocene with Homo- and Heterochiral Pro-Ala Sequences (**42–45**)

Encouraged by the results of conformational analysis and interesting chiroptical properties of **36–38** described above, we have synthesized four homo- and heterochiral aminoferrocene derived peptides: Boc-AA₂-AA₁-NH-Fn (**42**, AA₁ = L-Ala, AA₂ = L-Pro; **43**, AA₁ = D-Ala, AA₂ = D-Pro; **44**, AA₁ = L-Ala, AA₂ = D-Pro; **45**, AA₁ = D-Ala, AA₂ = L-Pro).^[82] The preferred conformation, according to thorough experimental and theoretical analysis, of homochiral

derivatives **42** and **43** in solution was β -turn-like structure (Figure 25b). As can be seen in Figure 25a, chiral information was transferred from this local secondary structure to a ferrocene chromophore giving rise to strong mirror-image signals in the visible region of the CD spectra of enantiomeric **42** and **43**.

The change of the chirality of the amino acid at the $i + 1$ position (Pro) caused a disruption of β -turn-like secondary structure in the derived heterochiral peptides **44** and **45**, as suggested by the CD and NMR spectroscopy analysis. Computational study proposed that lowest energy conformers of heterochiral derivatives were stabilized by two consecutive γ -turns in solution of aprotic solvents (Figure 25b).

On the contrary, the single-crystal X-ray structures of heterochiral Boc-D-Pro-L-Ala-NH-Fn (**44**) and Boc-L-Pro-D-Ala-NH-Fn (**45**) were characterized by the presence of 10-membered hydrogen-bond ring between NH adjacent to the ferrocene moiety and urethane carbonyl group (Figure 26). Intramolecular hydrogen bonding supported the formation of β -turn structure similar to an ideal type II β -turn. The right-handed sense of helical induction was observed in the structure of **45** while enantiomeric **44** favoured left-handed helical conformation.

Having in mind the results that clearly showed that the transfer of the chiral information from folded peptide chain to organometallic chromophore gives rise to strong response in the ferrocene region of CD spectra, our current research is focused on synthesis, conformational analysis and chiroptical properties of bioconjugates with a potential to form minimum sized peptide helices.

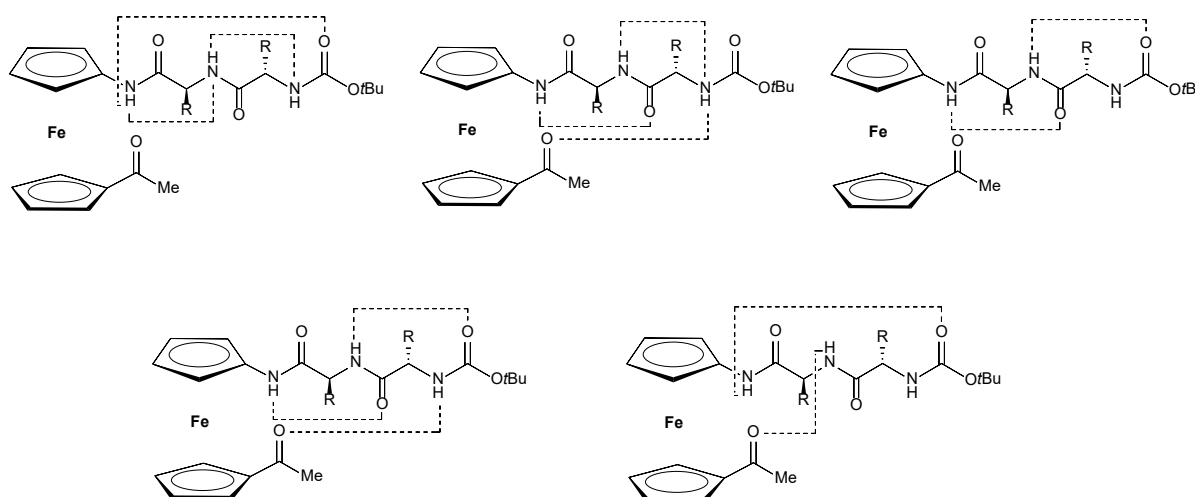


Figure 24. IHB patterns observed in the ensemble of the most stable conformers based on computational study for disubstituted conjugates **39–41**.

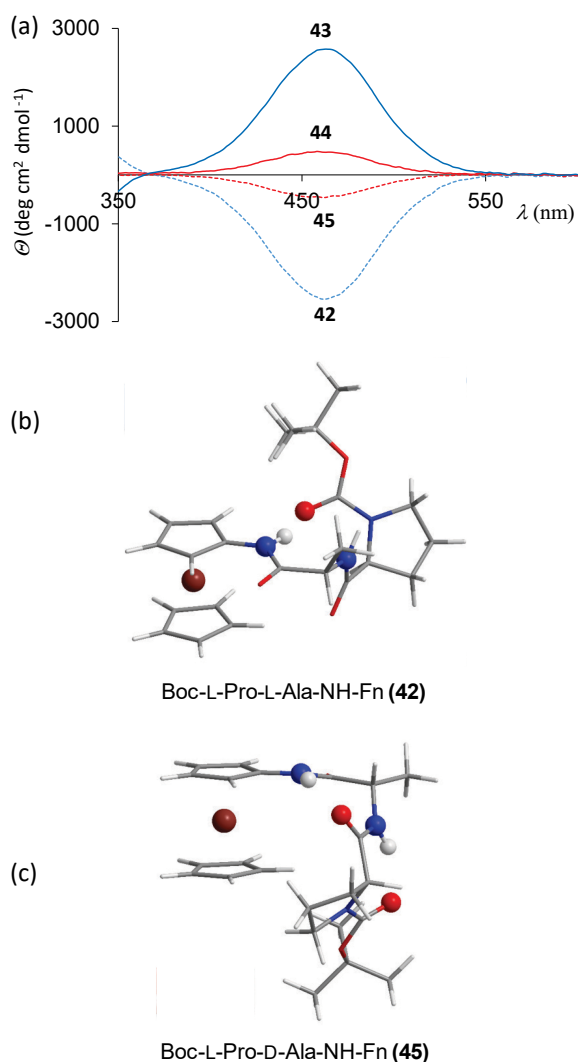


Figure 25. (a) Cotton effects in chirality-organized ferrocene peptides **42–45** in CH_2Cl_2 ($c = 1 \times 10^{-3}$ M), (b) β -turn structure in the most stable conformer of homochiral peptide **42** and (c) γ -turns in the heterochiral derivative **45**.

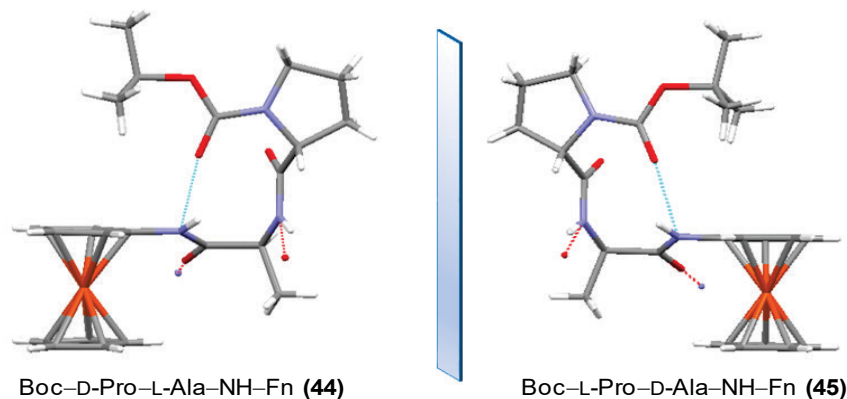


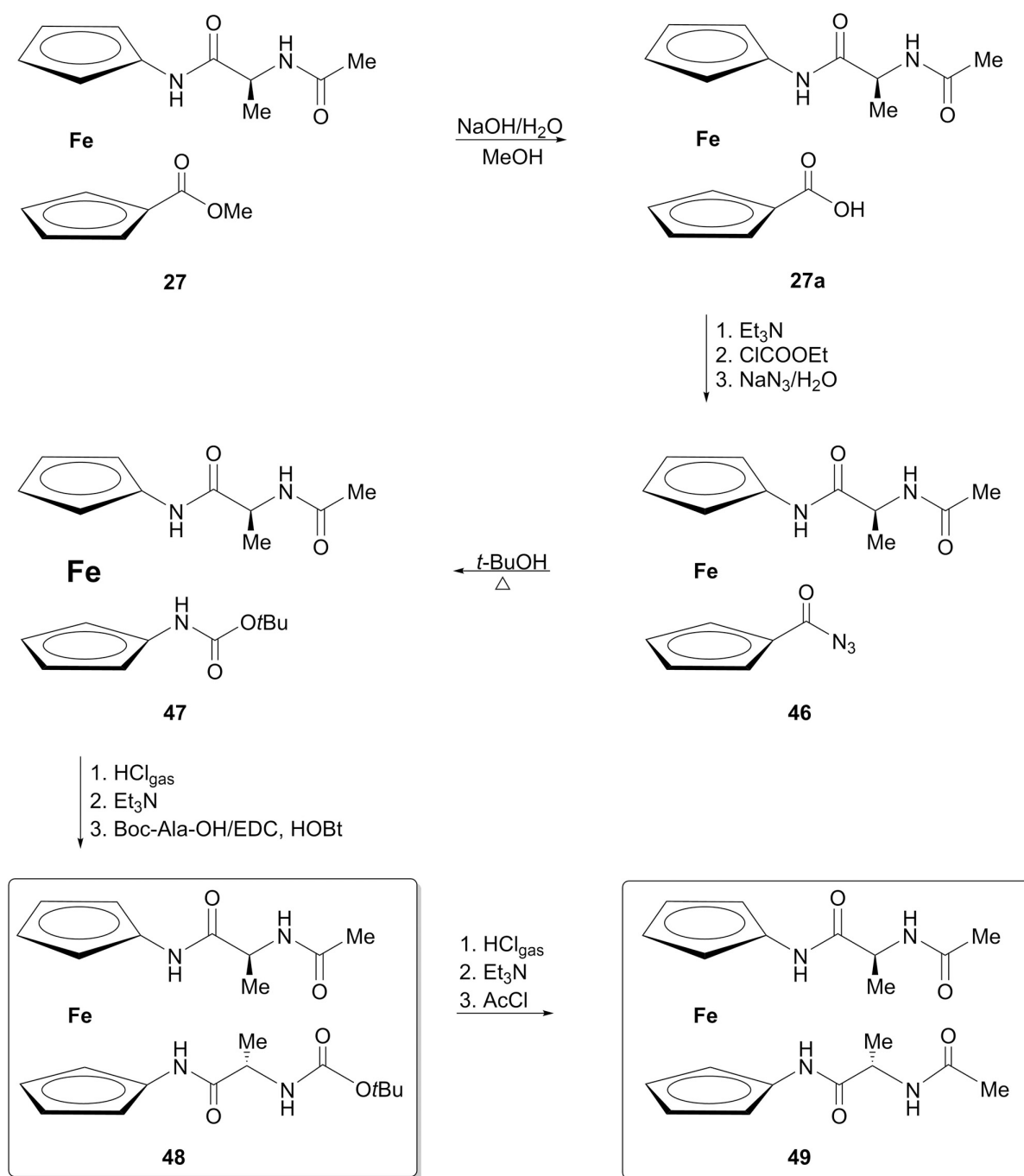
Figure 26. The enantiomeric β -turns in the crystal structures of heterochiral peptides **44** and **45**.

Biconjugates of Ferrocene-1,1'-diamine and Alanine (**48** and **49**)

Unlike peptides **III** and **IV** that have been widely reported, only one paper dealing with two symmetrically disubstituted homochiral peptides $\text{Fn}-(\text{NH-AA-Boc})_2$ (**Va**, AA = L- or D-Ala), derived from $\text{Fn}(\text{NH-Boc})_2$, was given by Kraatz *et al.*^[34] They have demonstrated that 14-membered ring between attached symmetrical peptide chains, very similar to those founded in antiparallel β -sheet peptides, was formed. Therefore, ferrocene-1,1'-diamine (Fcda) scaffold was established as a desired structural requirement for turn induction and mimicking the natural structure of antiparallel β -sheet. Within our recent research,^[83] we have designed a synthetic approach to unsymmetrically disubstituted and orthogonally protected conjugates $\text{Ac-Ala-NH-Fn-NH-Ala-Boc}$ (**48**) and $\text{Fn}-(\text{NH-Ala-Ac})_2$ (**49**) (peptides of type **V**), with aim to explore whether the replacement of one or both Boc groups of **Va** with sterically less demanding Ac groups in **48** and **49** will affect the IHB pattern realized through 14-membered $\text{NH}_{\text{Fn}} \cdots \text{OC}_{\text{Boc}}$ IHB ring.

The key intermediate **47**, containing NH groups attached to both Cp rings, was obtained from $\text{Ac-Ala-NH-Fn-COOMe}$ (**27**).^[74] The product obtained upon saponification of its ester group was transferred to orthogonally protected compound **47** *via* unstable azide **46**. Then, acidic Boc-deprotection of **47** and coupling with activated Boc-Ala-OH gave orthogonally protected $\text{Ac-Ala-NH-Fn-NH-Ala-Boc}$ (**48**). Upon (i) Boc-deprotection and (ii) Ac-protection in the presence of acetyl chloride,^[84] $\text{Fn}-(\text{NH-Ala-Ac})_2$ (**49**) was obtained (Scheme 7).

The both goal compounds displayed the similar IR behavior, based on dominant intramolecular hydrogen bonding engagement. Since the ratios of hydrogen-bonded and non-bonded NH peak intensities in their IR spectra were almost the same, the steric hindrance of Boc group was excluded.



Scheme 7. The synthesis of bioconjugates **48** and **49**.

The concentration-independent NMR data suggested the participation of downfield shifted NH_{Fn} of **48** and **49** in intramolecular HB, while NH_{Ac} protons experienced upfield shifting upon dilution, probably due to their involvement to a lesser extent in intermolecular HB. Therefore, the larger temperature dependencies of NH_{Fn} and NH_{Ac} were attributed to unfolding or dissociation of the initially shielded states, while the low temperature

dependence of upfield shifted NH_{Boc} corroborated its non-involvement in HB (Figure 27a). The titration with hydrogen-bond-accepting DMSO did not affect the chemical shifts of NH_{Fn} protons, suggesting their involvement in a strong IHBs. The pronounced changes in chemical shifts were observed for NH_{Ac} and NH_{Boc} ($\Delta\delta > 1.7$ ppm), confirming the proposed non-hydrogen-bonded state for NH_{Boc} as well as involvement of NH_{Ac} in a weak HB (Figure 27b).

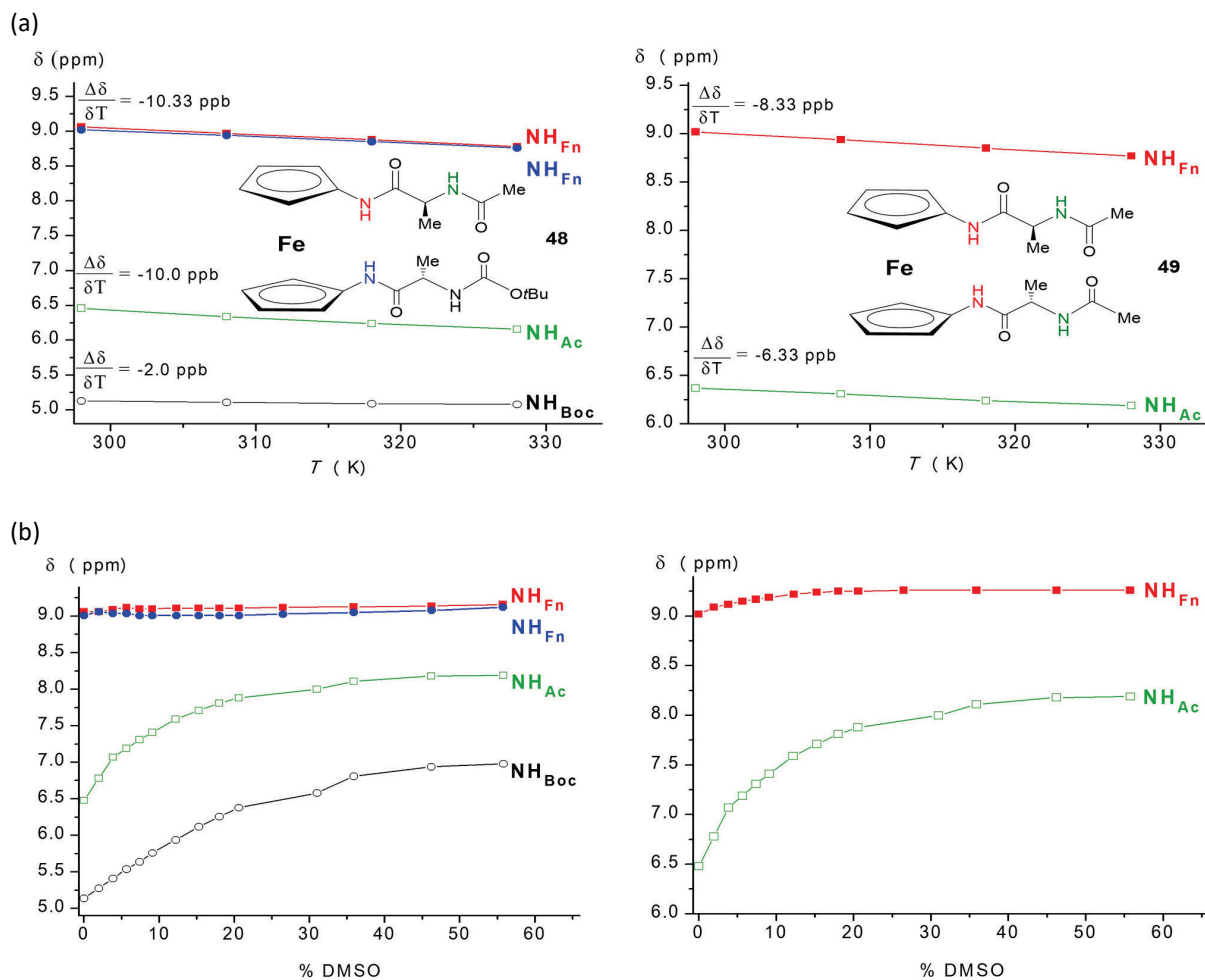


Figure 27. (a) Temperature dependence of NH chemical shifts of peptides **48** and **49** ($c = 2.5 \times 10^{-2}$ M) in the temperature range of 298–328 K, (b) Solvent dependence of NH chemical shifts of **48** and **49** at varying concentrations of d_6 -DMSO in $CDCl_3$ ($c = 2.5 \times 10^{-2}$ M, 298 K) to probe exposed vs. hydrogen-bonded amides.

These results contributed to define the conformational environment based on $NH_{Fn} \cdots OC_{Boc/Ac}$ IHBs. The interstrand NOE contact observed between NH_{Fn} linked at one Cp ring and tBu group belonging to the chain attached to another Cp ring supported the proposed interstrand intramolecular hydrogen bonding engagement and the presence of 14-membered ring (Figure 28a).

The observed strong Cotton effects in the region of ferrocene-based transitions around 470 nm supported the highly organized chiral surrounding around ferrocene unit. Considering that Cotton effect reflects an average of the entire molecular population, the prevalence of *P*-helicity was strongly supported. Furthermore, the conservation of $\sim 70\%$ of CD activity in the presence of 20% of DMSO was an additional confirmation of the involvement of the tested peptides in strong IHBs (Figure 28b).

The computational study of the bioconjugates **48**

and **49** confirmed the NMR proposed hydrogen bonding patterns. Thereat, the interchain $NH_{Fn} \cdots OC_{Boc/Ac}$ IHBs enabled the peptide chain to fold into β -turn-like structure (Figure 29).

The conformational pattern established in solution persisted in the solid state as well and it was accompanied by favorable intermolecular hydrogen bonds in the formation of infinite *zig-zag* chains (Figure 30).

The ferrocene conjugates **48** and **49** were screened *in vitro* for their potential anticancer activity in HepG2 human liver carcinoma cells and Hs578T human breast cancer cells (Figure 31). Although the both tested compounds were founded to adopt the same conformational pattern, the peptide **48** displayed the improved bioactivity, most likely due to its increased lipophilicity ($R_f = 0.51$) in comparison to the more polar **49** ($R_f = 0.12$).

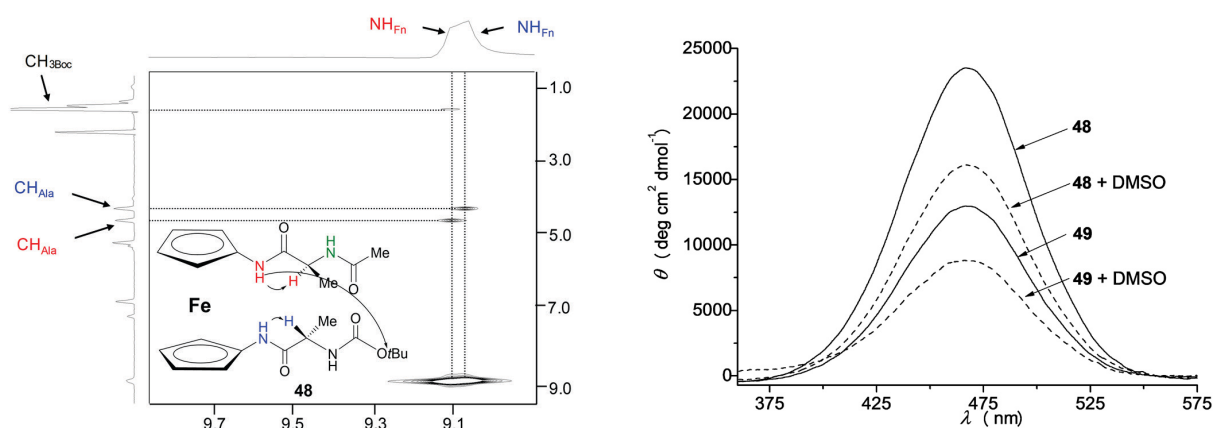


Figure 28. The interchain NOE connectivities between C- and N-termini of **48** (left) and Cotton effects in chirality-organized ferrocene peptides **48** and **49** in CH_2Cl_2 [(—) $c = 1 \times 10^{-3}$ M] and CH_2Cl_2 ($c = 1 \times 10^{-3}$ M) containing 20% of DMSO (---) (right).

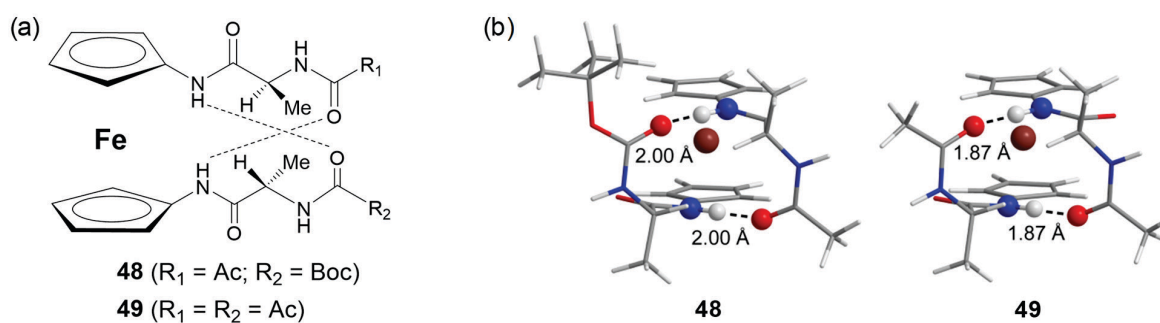


Figure 29. (a) IHB patterns and (b) optimized geometries of the most stable conformers based on computational study for peptides **48** and **49**.

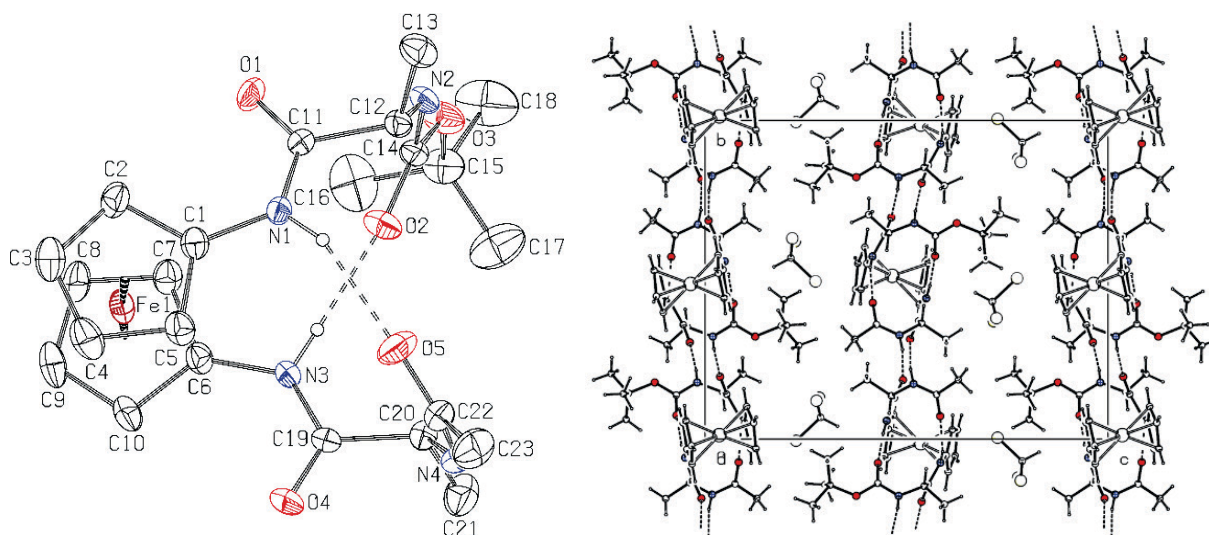


Figure 30. A molecular structure of bioconjugate **48** (left) and crystal packing diagram showing intramolecular and intermolecular N-H...O hydrogen bonds (right).

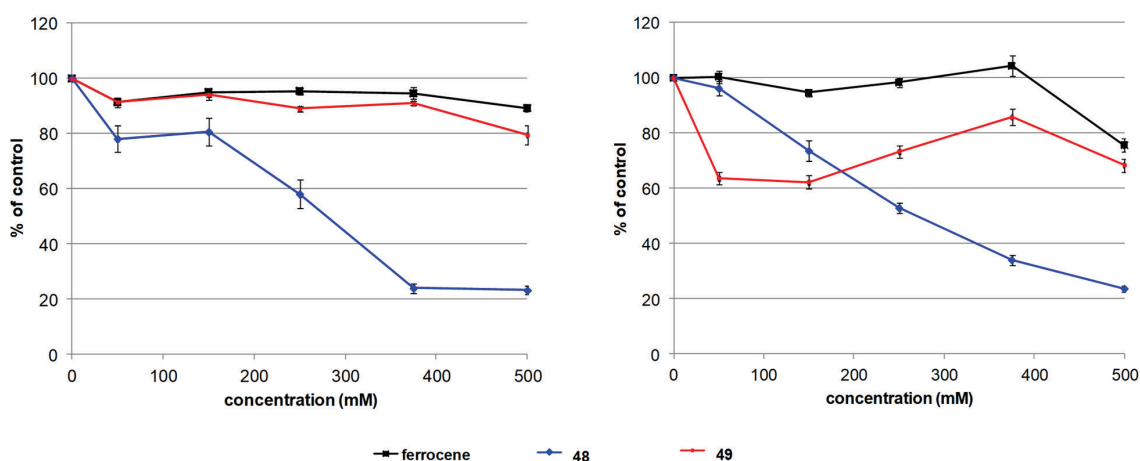


Figure 31. *In vitro* anti-proliferative effect of ferrocene and ferrocene conjugates **48** and **49** against HepG2 human liver carcinoma cells (left) and Hs578T human breast cancer cells (right). The lines connecting the measured points are drawn to enhance clarity.

Bioconjugates of Ferrocene-1,1'-diamine with Homo- and Heterochiral Pro-Ala Sequences (**62–65** and **69–72**)

Recently, we reported the synthesis of the peptides **62–65** and **69–72** that contain Ala-Pro sequences coupled to NH-derivatized cyclopentadienyl (Cp) rings.^[36] In order to examine the influence of the backbone chirality and *N*-terminal groups on conformational properties, the synthesized peptides were designed to contain homo- or heterochiral Ala-Pro sequences with different *N*-terminal groups *i.e.* the bulky Boc or sterically less demanding Ac functionality.

The peptides **62–65** were prepared by using the same synthetic approach applied for the synthesis of their lower homologues **48** and **49** (Scheme 8), while the symmetrically disubstituted peptides **69–72** were prepared following the procedure applied for the synthesis of their lower homologues **Va**^[34] (Scheme 9).

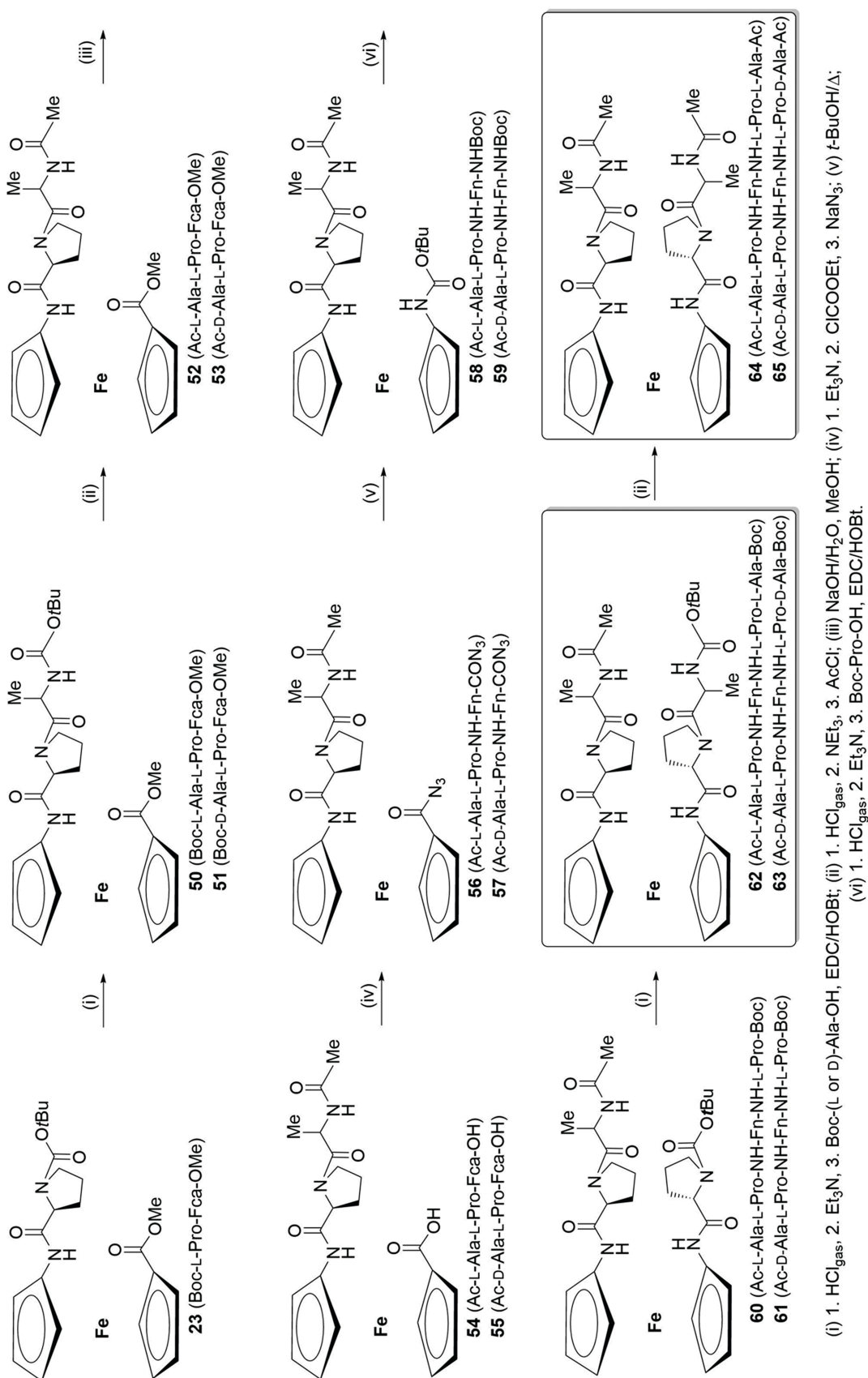
The capacity for turn formation was explored by concentration-dependent IR spectroscopy and concentration-, temperature- and solvent-dependent NMR studies. The distinct bands at $\sim 3430\text{ cm}^{-1}$ and $\sim 3250\text{--}3300\text{ cm}^{-1}$ in solution state IR spectra of the examined peptides suggested the presence of both free and associated NH groups. The blue-shifted amide I bands ($\sim 1710\text{ cm}^{-1}$) observed in IR spectra of Boc-peptides **62**, **63** and **72** suggested the alteration of the conformational properties in comparison to Ac-peptides **64** and **65**. The relative intensities of free and associated amide bands of the tested peptides were maintained during dilution, owing to the intramolecular engagement of hydrogen-bonded amide groups.

The two kinds of resonances were observed in NMR spectra of the goal compounds: the downfield shifted

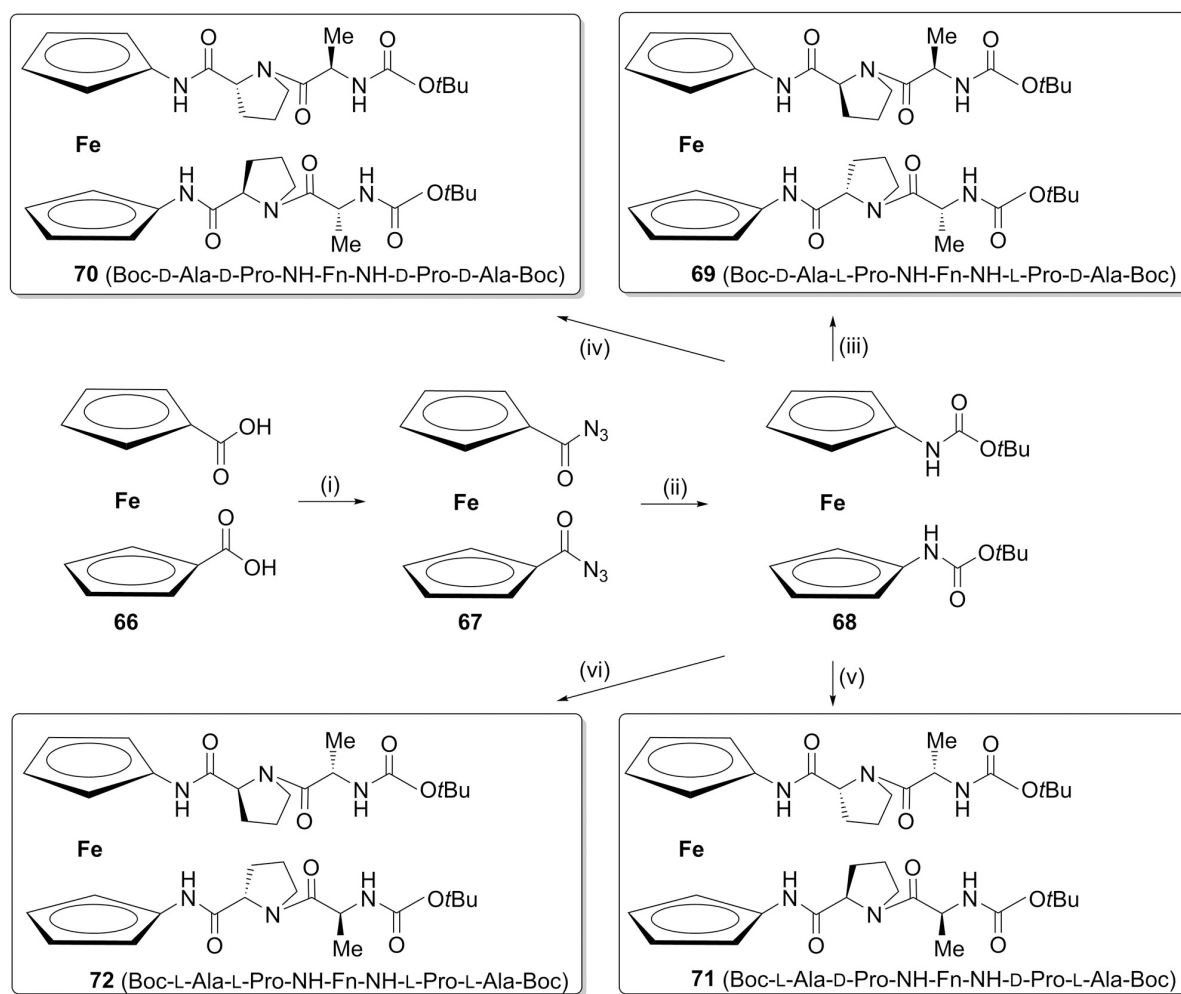
resonances of NH_{Fn} groups ($\delta \geq 9.2\text{ ppm}$) that suggested their involvement in HB and upfield shifted resonances of Ala- $\text{NH}_{\text{Boc/Ac}}$ ($\delta \sim 5\text{--}6.5\text{ ppm}$) that suggested the lower potential to experience hydrogen-bonding.

The IR findings on non-involvement of the examined peptides in intermolecular aggregation were supported by the sharp signals and non-affected (NH_{Fn} and Ala- NH_{Boc}) or slightly affected chemical shifts (Ala- NH_{Ac}) upon dilution up to 50-fold (Figure 32a). Furthermore, no significant upfield shift of the amide protons was observed upon successive heating of 1 mM solutions of the examined peptides in CDCl_3 in the range of 258–328 K, certainly due to their involvement in strong IHBs or non-involvement in hydrogen bonding at all (Figure 32b). While the amide resonances belonging to the conformers of the homochiral peptides remained resolved at increased temperature, the signals of heterochiral peptides underwent partial coalescence, suggesting conformational differences imparted by backbone chirality.

The larger temperature dependencies of the concentration-independent NH_{Fn} protons of peptides **62–65** indicated that they were initially shielded owing to the hydrogen bonding engagement, but became exposed to the solvent upon unfolding of the ordered structures at increased temperatures. The distinct conformational patterning of homo- and heterochiral peptides was strongly suggested by different temperature dependencies (Figure 32b). The concentration-independent D-Ala- NH_{Ac} in heterochiral peptides **63** and **65** exhibited the larger temperature dependencies due to their participation in intramolecular hydrogen bonding. At the same time, the smaller temperature dependencies of the upfield shifted L-Ala- NH_{Ac} in homochiral peptides **62** and **64** reflect their non-involvement in HBs (Figure 33).



Scheme 8. Synthesis of orthogonally protected ferrocene-peptide conjugates **62** and **63** and their corresponding Ac-analogues **64** and **65** containing homo- and heterochiral Ala-Pro sequences.



- (i) 1. Et₃N, 2. ClCOEt, 3. NaN₃; (ii) *t*-BuOH/ ; (iii) 1. TFA, 2. Et₃N, 3. Boc-D-Ala-L-Pro-OH, HBTU/HOBt;
 (iv) 1. TFA, 2. Et₃N, 3. Boc-D-Ala-D-Pro-OH, HBTU/HOBt; (v) 1. TFA, 2. Et₃N, 3. Boc-L-Ala-D-Pro-OH, HBTU/HOBt;
 (vi) 1. TFA, 2. Et₃N, 3. Boc-L-Ala-L-Pro-OH, HBTU/HOBt.

Scheme 9. Synthesis of symmetrically disubstituted ferrocene-peptide conjugates **69–72** containing homo- or heterochiral Ala-Pro sequences.

The different conformational behaviour of intramolecularly engaged NH_{F_n} protons of homo- and heterochiral peptides was additionally supported by DMSO titration experiments (Figure 34). While the NH_{F_n} protons of the homochiral peptides **62**, **64** and **72** moved slightly downfield in the presence of DMSO, the NH_{F_n} protons of the heterochiral peptides **63** and **65** moved slightly upfield. A common feature of their Ala-NH_{Boc/Ac} groups was a solvent exposure observable through a high degree of solvent sensitivity ($\Delta\delta \sim 1.28 - 1.9$) that emerged from their non-involvement in hydrogen bonding or involvement in only weak hydrogen bonds. Moreover, unlike the heterochiral counterparts, the portion of the *trans/trans* conformers of the homochiral peptides remained almost unchanged upon addition of DMSO.

Although the amide resonances of homo- and heterochiral peptides displayed different temperature and solvent dependences, their common conformational feature was involvement of NH_{F_n} protons in IHBs. Bearing in mind the number and position of hydrogen-bond accepting carbonyl groups, the tentative conformations of the examined peptides could, therefore, rely on both intra- and interstrand IHBs. The interstrand NOE contacts observed in spectra of orthogonally protected peptides **62** (NH_{F_n^b→Ala-NH_{Ac}) and **63** (NH_{F_n^b→Ala-NH_{Ac} and NH_{F_n^a→Ala-NH_{Boc}) corroborated the presence of interstrand IHBs. However, the NOE contacts NH_{F_n}→Me_{Ac} and NH_{F_n}→Ala-NH_{Ac} detected in spectra of symmetrically disubstituted Ac-protected peptides **64** and **65**, and}}}

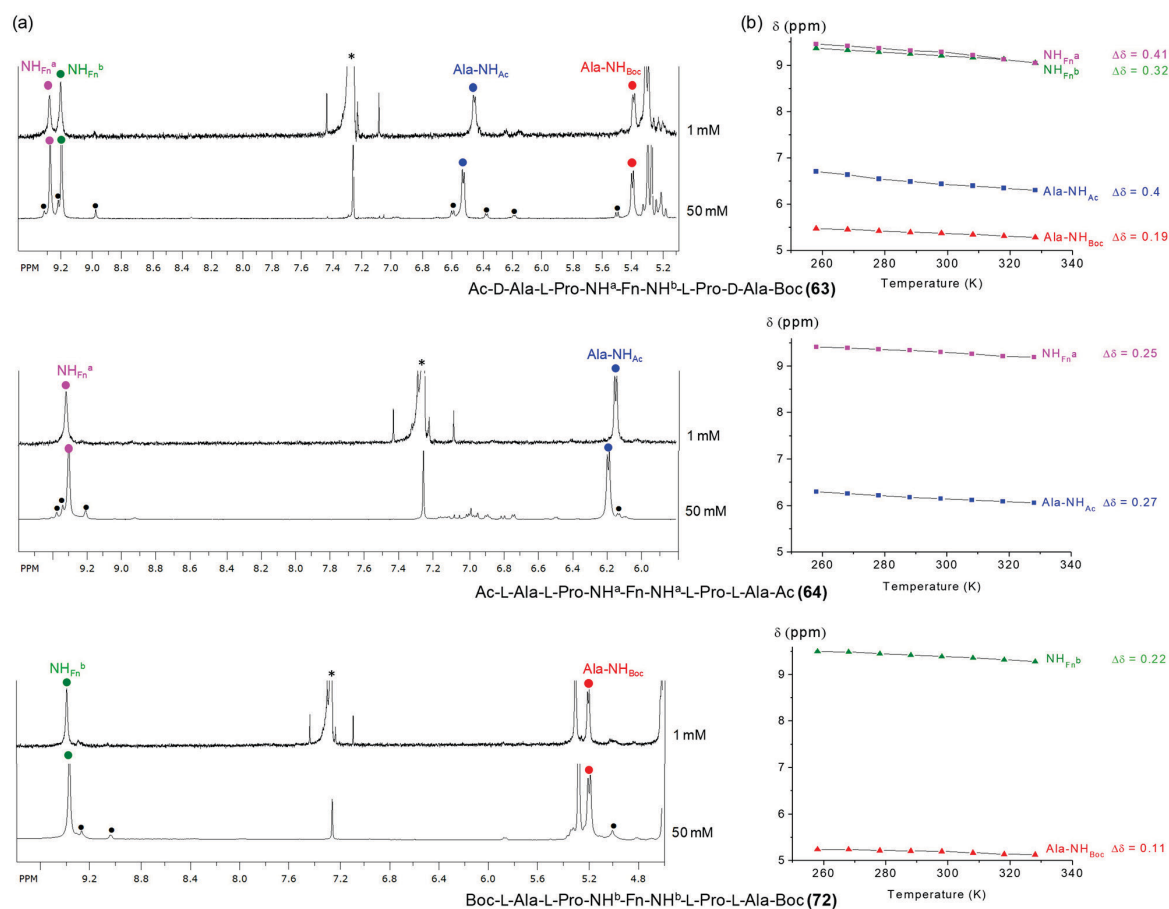


Figure 32. (a) Concentration dependence of NH chemical shifts of heterochiral peptide **63** and homochiral peptides **64** and **72** (* residual CDCl₃, • *trans/cis*, *cis/trans* and *cis/cis* rotamers), (b) Temperature dependence of NH chemical shifts of heterochiral and orthogonally protected peptide **63** and homochiral peptides **64** and **72** ($c = 1 \times 10^{-3}$ M in CDCl₃) in the temperature range of 258–328 K. The corresponding chemical shift differences ($\Delta\delta$) are indicated on the right.

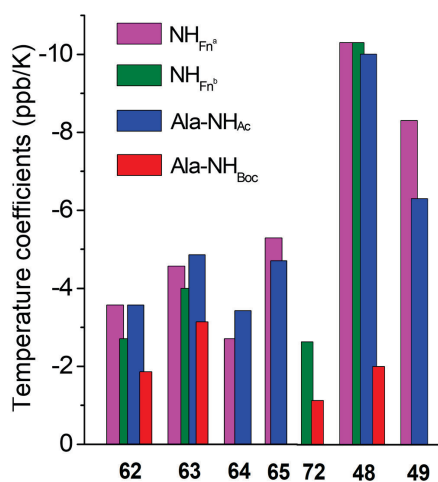


Figure 33. Amide temperature coefficients of the homochiral peptides **62**, **64** and **72**, heterochiral peptides **63** and **65** and their lower homologues **48** and **49** ($c = 1 \times 10^{-3}$ M in CDCl₃).

NH_{Fn}→Ala-NH_{Boc} visible in spectrum of symmetrically disubstituted Boc-protected peptide **72**, might account for both intra- and interstrand IHBs (Figure 35).

The strong positive Cotton effects observed in CD spectra of the examined compounds strongly suggested the high level of chiral organization *i.e.* *P*-helicity, established through interstrand hydrogen bonding (Figure 36). The different loss of CD activity in the presence of 50 % of DMSO indicated the different hydrogen bonds strength. The heterochiral peptide **65**, founded to be the most solvent-exposed due to the largest DMSO-induced shift of its amide protons, conserved only 35 % of initial CD activity. Similarly, the other tested heterochiral peptide **63** maintained 39 % of its CD activity. The homochiral peptides **64** and **72** were founded to be more stable, preserving 57–89 % of the initial CD activity upon addition of 50 % of DMSO.

The quite different DMSO-behaviour of concentration- and temperature-independent NH_{Fn} protons of homo- (**62**, **64**, **72**) and heterochiral peptides (**65**) implied the different

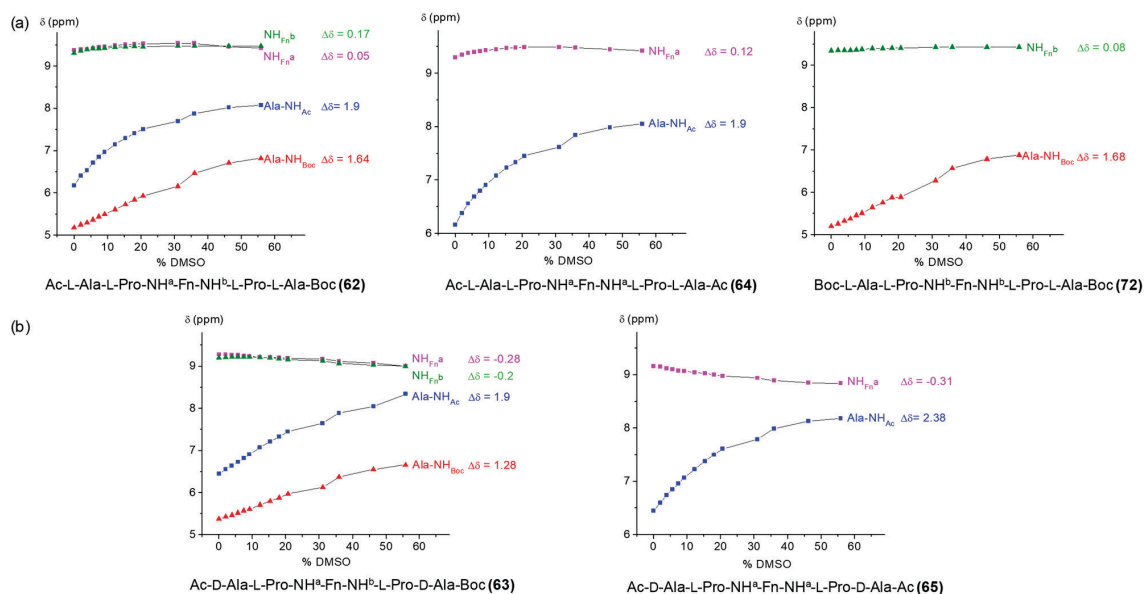


Figure 34. Solvent dependence of NH chemical shifts of (a) homochiral peptides **62**, **64** and **72** and (b) heterochiral peptides **63** and **65** at increasing concentrations of d_6 -DMSO in $CDCl_3$ ($c = 25$ mM, 298 K) to probe exposed vs. hydrogen-bonded amides.

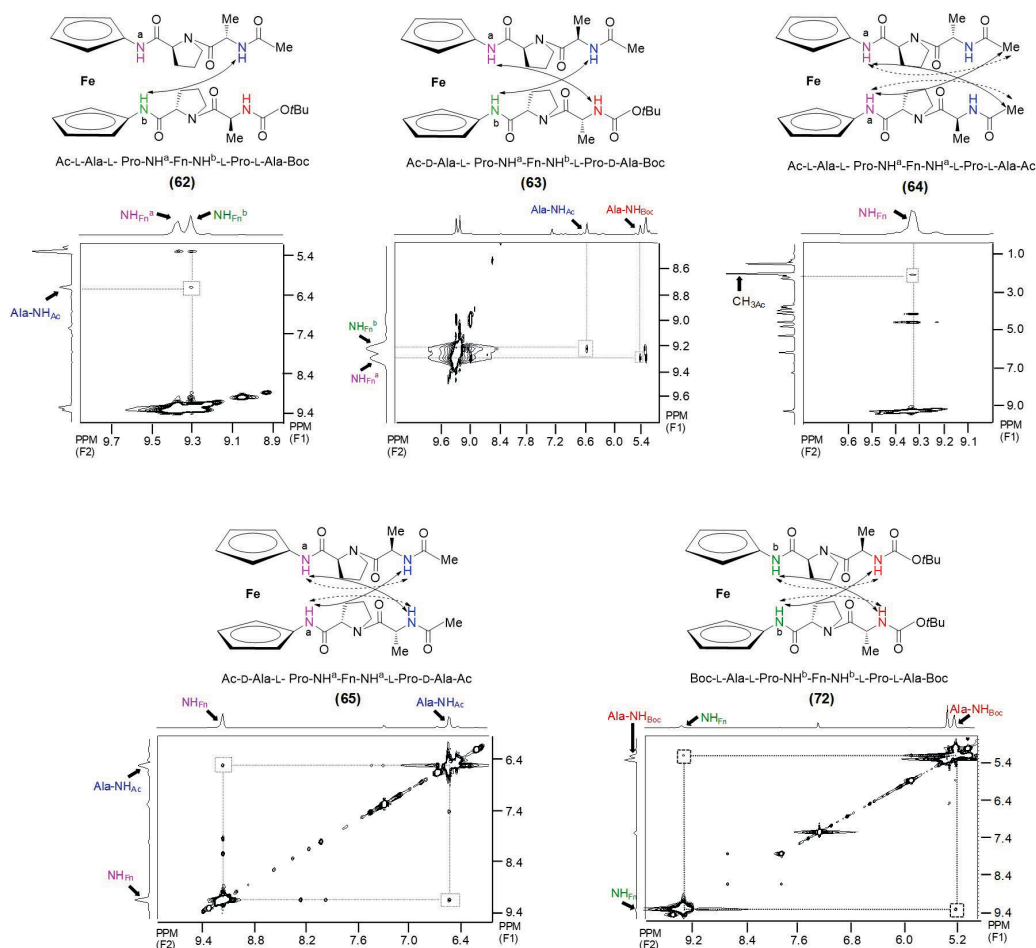


Figure 35. The interstrand NOE connectivities in spectra of **62–65** and **72** are depicted with arrows.

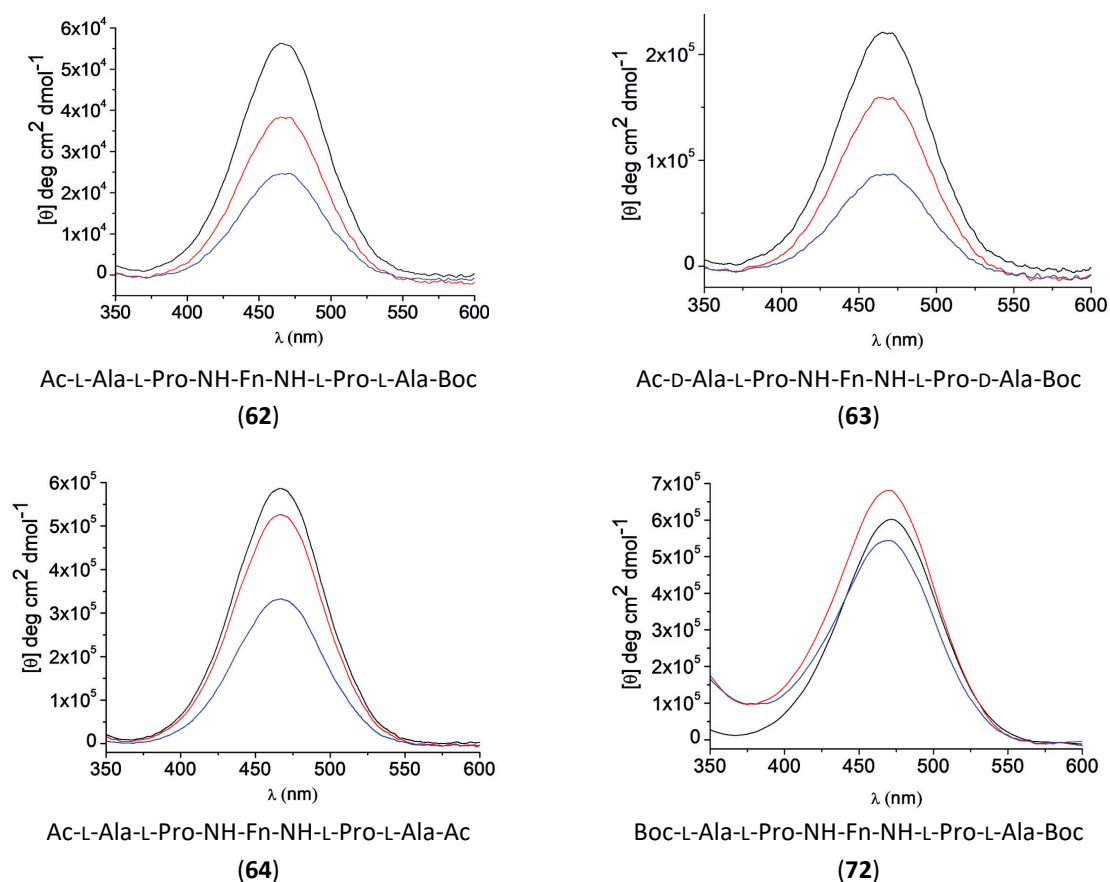


Figure 36. The Cotton effects in chirality-organized ferrocene peptides **62–64** and **72** in solution {CH₂Cl₂ [(–) $c = 1 \times 10^{-3}$ M], CH₂Cl₂ ($c = 1 \times 10^{-3}$ M) containing 20 % of DMSO (—) and CH₂Cl₂ ($c = 1 \times 10^{-3}$ M) containing 50 % of DMSO (—)}.

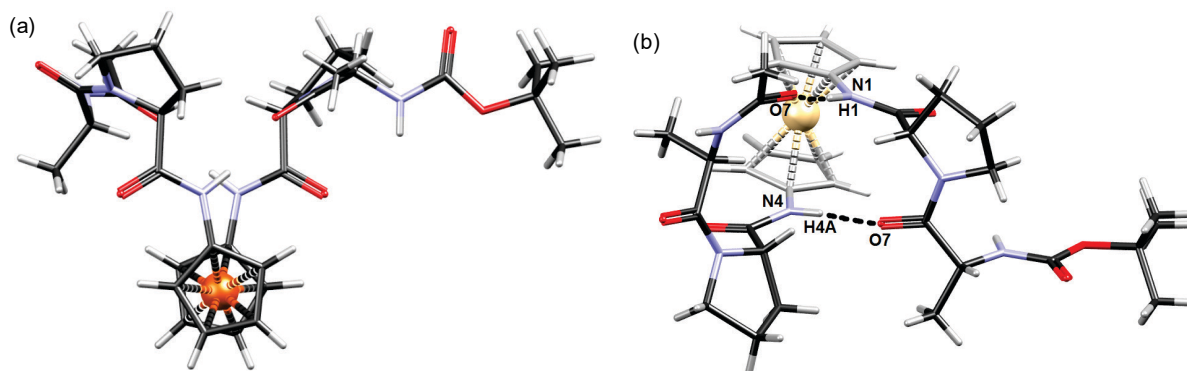


Figure 37. Conformation of Ac-D-Ala-L-Pro-NH-Fn-NH-L-Pro-D-Ala-Boc (**63**). (a) top-down view revealing *P*-helicity and torsion between peptide chains, (b) a side-view showing conformation of peptide chains stabilized by IHBS.

conformational patterns established through IHBS of different kinds and strength. Considering that the less stable conformations arose if the hydrogen bonds were established within the same strand,^[74,77] the engagement of DMSO-sensitive NH_{Fn} of peptide **65** in intrastrand IHBS was strongly suggested.

The *P*-helicity indicated by CD data was also determined in the crystal structure of compound **63**. The two IHBS between the podant peptide strands forming one ten-membered (β -turn-like) and one thirteen-membered ring were observed (Figure 37).

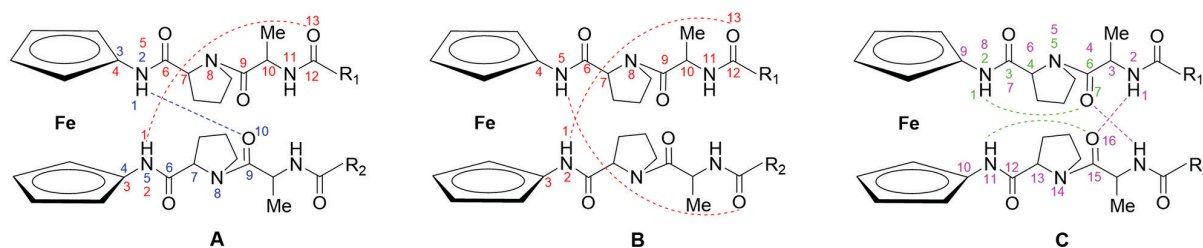


Figure 38. The intramolecular hydrogen bonding patterns observed in homochiral peptides **62**, **64** and **72** (patterns **A** and **B**) and heterochiral peptides **63** and **65** (pattern **C**). **62** and **63** ($R_1 = \text{Me}$, $R_2 = \text{OtBu}$), **64** and **65** ($R_1 = R_2 = \text{Me}$), **72** ($R_1 = R_2 = \text{OtBu}$). Numerations of the corresponding hydrogen bonded rings are displayed.

The DFT study corroborated the different conformational behaviour suggested by spectroscopic analyses (Figure 38). The homochiral peptides **62**, **64** and **72** were prone to form simultaneous intramolecular hydrogen bonding engagement of NH_{Fn} , influenced by the steric bulkiness of the *N*-terminal group. The Ac-derivative **64** adopted the two thirteen-membered interstrand hydrogen bonded rings (pattern **B**). In the peptides **62** and **72**, containing one or both bulky Boc-groups instead of Ac, one thirteen-membered hydrogen bonded ring was preserved while another was replaced with ten-membered ring (pattern **A**).

The L- to D-Ala exchange in heterochiral peptides **63** and **65** strongly influenced their conformational patterning: the thirteen-membered ring, most commonly observed in the heterochiral counterparts, was replaced by the highly symmetrical intramolecular hydrogen bonding pattern made of seven-membered intrastrand and sixteen-membered interstrand hydrogen bonds (pattern **C**).

Considering the revealed turn-inducing potential of Fcda scaffold, our future work will be directed to the conjugates of Fcda with biologically valuable branched-chain amino acids.

CONCLUSIONS

This review is aimed to underline the biological and conformational potential of ferrocene bioconjugates synthesized in our group. Although we have been mainly focused on the conformational behaviour of ferrocene peptidomimetics, the attention was also paid to the potentially biologically active ferrocene compounds. The biological evaluation revealed both the cytotoxic and hemagglutination inhibition potential of ferrocene bioconjugates. The conjugation of resveratrol with ferrocene was shown to contribute to the improved cytotoxicity against liver cancer cells HepG2, whilst significantly lower cytotoxicity on normal ovary CHO-K1 cells was observed. The interesting biological phenomenon named hormesis was observed for oxalamide-bridged

ferrocene which displayed proliferative effect on normal kidney HEK293T cells followed with cytotoxic activity against tumour cervical HeLa cells. Besides the cytotoxic activity, ferrocenes were also tested as inhibitors of FimH-mediated hemagglutination. Among the so far tested ferrocene conjugates with mannopyranoside acid, equipped with aglycon alkyl chains of different length ($n = 0-5$), the most pronounced increment of inhibitory activity was observed for those which contains butyl group.

The major part of our research was aimed to study the conformational behaviour of ferrocene peptidomimetics. For that purpose, three different ferrocene scaffolds ($-\text{NH}-\text{Fn}$, $-\text{NH}-\text{Fn}-\text{CO}-$ and $-\text{NH}-\text{Fn}-\text{NH}-$) were employed to conjugate with various amino acid sequences and the obtained peptides were subjected to detailed conformational analysis based on spectroscopic measurements (IR, NMR and CD) and DFT study.

The results of conformational analysis of peptides **25-28** [$\text{Y}-\text{L-Ala}-\text{NH}-\text{Fn}-\text{COOMe}$ (**25**, $\text{Y} = \text{Boc}$; **27**, $\text{Y} = \text{Ac}$) and $\text{Y}-\text{D-Ala}-\text{NH}-\text{Fn}-\text{COOMe}$ (**26**, $\text{Y} = \text{Boc}$; **28**, $\text{Y} = \text{Ac}$)] suggested the presence of *intra*- [7-membered $\text{NH}_{\text{Fn}} \cdots \text{N}_{\text{Ala}}$ HB-ring (γ -turn) and 5-membered $\text{NH}_{\text{Fn}} \cdots \text{N}_{\text{Ala}}$ HB-ring] and interstrand IHBs (9-membered $\text{NH}_{\text{Ala}} \cdots \text{O}_{\text{Fn}}$ HB-ring). The alanine chirality was not observed to influence the hydrogen bonding patterning, while the presence of Boc group was founded to interfere with hydrogen bonding to a lesser extent. The results of computational analysis corroborated the IHB motifs predicted by experimental data.

The medium-strength hydrogen bond, established between NH_{Fn} and urethane carbonyl, was found in the lowest homologues of nonsymmetric ferrocene peptides **33-35** (Boc-AA-NH-Fn-COMe ; $\text{AA} = \text{Gly}$, L-Ala, L-Val) and their monosubstituted analogues **30-32** (Boc-AA-NH-Fn ; $\text{AA} = \text{Gly}$, L-Ala, L-Val). *N*-terminal elongation of **30-35** gave mono- **36-38** [$\text{Boc}-(\text{AA})_2-\text{NH-Fn}$; $\text{AA} = \text{Gly}$, L-Ala, L-Val] and disubstituted ferrocene peptides **39-41** [$\text{Boc}-(\text{AA})_2-\text{NH-Fn-COMe}$; $\text{AA} = \text{Gly}$, L-Ala, L-Val]. According to computational analysis, the lowest energy conformer of monosubstituted derivatives **36-38** is stabilized by β -turn-like structure (10-membered $\text{NH}_{\text{Fn}} \cdots \text{O}_{\text{Boc}}$ HB ring).

Additional hydrogen bond acceptor group (COMe) in the analogous 1-acetyl derivatives (**39–41**) enables them to form interchain hydrogen bonds and causes the destabilization of β -turn structures.

While the enantiomeric β -turns were found to be most stable conformations of homochiral derivatives Boc-AA₂-AA₁-NH-Fn (**42**, AA₁ = L-Ala, AA₂ = L-Pro; **43**, AA₁ = D-Ala, AA₂ = D-Pro), the change of the chirality of the amino acid at the *i* + 1 position of β -turn causes its disruption in the solutions of the derived heterochiral peptides **44** (AA₁ = L-Ala, AA₂ = D-Pro) and **45** (AA₁ = D-Ala, AA₂ = L-Pro) as suggested by the CD, NMR spectroscopy and theoretical analysis.

Ferrocene-1,1'-diamine scaffold was found to induce the formation of two simultaneous 10-membered β -turn-like structures in peptides Ac-Ala-NH-Fn-NH-Ala-Boc (**48**) and Fn-(NH-Ala-Ac)₂ (**49**), thus replicating hydrogen bonding pattern of peptide β -sheets. The same pattern was established in the solid state and was corroborated with DFT data.

The different conformational behaviour of homo- (**62**, **64** and **72**) and heterochiral peptides (**63** and **65**) comprised of -NH-Fn-NH- scaffold and Ala-Pro sequences was strongly suggested by spectroscopic analyses and corroborated with DFT studies. The Ac-derivative **64** adopted the two 13-membered NH_{Fn}...OC_{Ac} interstrand hydrogen bonded rings. In the peptides **62** and **72**, that contain one or both bulky Boc-groups instead of Ac, one 13-membered hydrogen bonded ring was preserved while another was replaced with 10-membered interstrand ring (NH_{Fn}...OC_{Ala}). Upon L- to D-Ala exchange, the 13-membered ring, most commonly observed in the heterochiral conjugates, was replaced by the highly symmetrical intramolecular hydrogen bonding pattern made of two pairs of hydrogen bonds, 7-membered intrastrand NH_{Fn}...OC_{Ala} and 16-membered interstrand NH_{Fn}...OC_{Ala} hydrogen bonds. The relationship observed between the backbone homo- or heterochirality, the hydrogen bonding acceptor ability of the *N*-terminal groups and the hydrogen bonding patterning can be applied to tune the preferred hydrogen bonded ring size in the derived peptidomimetics.

Acknowledgments. We would like to express sincere gratitude to our supervisor Vladimir Rapić and advisors Srđanka Tomić and Mladen Žinić for introducing us into the subject. We also thank to our colleagues who contributed as co-authors to the joint researches. This work was supported by a grant from Croatian Science Foundation (project IP-2014-09-7899).

REFERENCES

- [1] T. J. Kealy, P. L. Pauson, *Nature* **1951**, *168*, 1039.
- [2] G. Wilkinson, M. Rosenblum, M. C. Whiting, R. B. Woodward, *J. Am. Chem. Soc.* **1952**, *74*, 2125.
- [3] R. B. Woodward, M. Rosenblum, M. C. Whiting, *J. Am. Chem. Soc.* **1952**, *74*, 3458.
- [4] H. Werner, *Angew. Chem. Int. Ed.* **2012**, *51*, 2.
- [5] D. Astruc, *Eur. J. Inorg. Chem.* **2017**, 6.
- [6] A. E. G. Cass, G. Davies, G. D. Francis, H. A. O. Hill, W. J. Aston, J. Higgins, E. V. Plotkin, L. D. L. Scott, A. P. F. Turner, *Anal. Chem.* **1984**, *56*, 667.
- [7] M. Salmain, *Labeling of Proteins with Organometallic Complexes: Strategies and Applications, in Bioorganometallics. Biomolecules, Labelling, Medicine* (Ed. G. Jaouen), Wiley-VCH Verlag GmbH & Co. KGaA, Weinheim, **2006**, 181.
- [8] a) G. Gasser, N. Metzler-Nolte, *Curr. Opin. Chem. Biol.* **2012**, *16*, 84; b) M. Patra, G. Gasser, *Nat. Rev. Chem.* **2017**, *1*, 0066.
- [9] V. N. Babin, Yu. A. Belousov, V. I. Borisov, V. V. Gumenyuk, Yu. S. Nekrasov, L. A. Ostrovskaya, I. K. Sviridova, N. S. Sergeeva, A. A. Simenel, L. V. Snegur, *Russ. Chem. Bull. Int. Ed.* **2014**, *63*, 2405.
- [10] G. Jaouen, A. Vessières, S. Top, *Chem. Soc. Rev.* **2015**, *44*, 8802.
- [11] S. Top, A. Vessières, G. Leclercq, J. Quivy, J. Tang, J. Vaissermann, M. Huche, G. Jaouen, *Chem. Eur. J.* **2003**, *9*, 5223.
- [12] A. A. Simenel, E. A. Morozova, L. V. Snegur, S. I. Zykova, V. V. Kachala, L. A. Ostrovskaya, N. V. Bluchterova, M. M. Fomina, *Appl. Organomet. Chem.* **2009**, *23*, 219.
- [13] A. D. S. Krishna, G. Panda, A. K. Kondapi, *Arch. Biochem. Biophys.* **2005**, *438*, 206.
- [14] B. Balaji, B. Balakrishnan, S. Perumalla, A. A. Karande, A. R. Chakravarty, *Eur. J. Inorg. Chem.* **2015**, 1398.
- [15] S. B. Deepthi, R. Trivedi, L. Giribabu, P. Sujitha, C. G. Kumar, *Dalton Trans.* **2013**, *42*, 1180.
- [16] E. I. Edwards, R. Epton, G. Marr, *J. Organomet. Chem.* **1976**, *107*, 351.
- [17] E. I. Edwards, R. Epton, G. Marr, *J. Organomet. Chem.* **1979**, *168*, 259.
- [18] D. Scutaru, L. Tataru, I. Mazilu, E. Diaconu, T. Lixandru, C. Simionescu, *J. Organomet. Chem.* **1991**, *401*, 81.
- [19] D. Scutaru, I. Mazilu, M. Vata, L. Tataru, A. Vlase, T. Lixandru, C. Simionescu, *J. Organomet. Chem.* **1991**, *401*, 87.
- [20] L. V. Snegur, V. N. Babin, A. A. Simenel, Yu. S. Nekrasov, L. A. Ostrovskaya, N. S. Sergeeva, *Russ. Chem. Bull. Int. Ed.* **2010**, *59*, 2167.
- [21] D. R. van Staveren, N. Metzler-Nolte, *Chem. Rev.* **2004**, *104*, 5931.
- [22] H.-B. Kraatz, *J. Inorg. Organomet. Polym. Materials* **2005**, *15*, 83.
- [23] E. W. Neuse, *J. Inorg. Organomet. Polym. Materials* **2005**, *15*, 3.

- [24] S. Top, J. Tang, A. Vessières, C. Carrez, C. Provot, G. Jaouen, *Chem. Commun.* **1996**, 955.
- [25] G. Jaouen, S. Top, A. Vessières, G. Leclercq, J. Quivy, L. Jin, A. Croisy, *C. R. Acad. Sci., Ser. IIc: Chim.* **2000**, *3*, 89.
- [26] D. Dive, C. Biot, *ChemMedChem.* **2008**, *3*, 383.
- [27] P. Štěpnička, *Ferrocenes: Ligands, Materials and Biomolecules*, John Wiley, Chichester, **2008**.
- [28] R. Ribić, M. Kovačević, V. Petrović-Peroković, I. Gruić-Sovulj, V. Rapić, S. Tomić, *Croat. Chem. Acta* **2010**, *83*, 421.
- [29] M. Kovačević, L. Barišić, R. Ribić, V. Petrović Peroković, S. Tomić, V. Rapić, *Appl. Organometal. Chem.* **2012**, *26*, 74.
- [30] G. Zhou, W. J. Mo, P. Sebbel, G. Min, T. A. Neubert, R. Glockshuber, X. R. Wu, T. T. Sun, X. P. Kong, *J. Cell. Sci.* **2001**, *114*, 4095.
- [31] M. Hartmann, T. K. Lindhorst, *Eur. J. Org. Chem.* **2011**, 3583.
- [32] a) A. Nomoto, T. Moriuchi, S. Yamazaki, A. Ogawa, T. Hirao, *Chem. Commun.* **1998**, 1963; b) T. Moriuchi, A. Nomoto, K. Yoshida, A. Ogawa, T. Hirao, *J. Am. Chem. Soc.* **2001**, *123*, 68; c) T. Moriuchi, T. Nagai, T. Hirao, *Org. Lett.* **2005**, *7*, 5265; d) T. Moriuchi, T. Nagai, T. Hirao, *Org. Lett.* **2006**, *8*, 31; e) T. Moriuchi, A. Nomoto, K. Yoshida, T. Hirao, *J. Organomet. Chem.* **1999**, *589*, 50; f) T. Moriuchi, A. Nomoto, K. Yoshida, T. Hirao, *Organometallics* **2001**, *20*, 1008; g) T. Moriuchi, T. Hirao, *Acc. Chem. Res.* **2010**, *43*, 1040; h) B. Adhikari, A. J. Lough, B. Barker, A. Shah, C. Xiang, H.-B. Kraatz, *Organometallics* **2014**, *33*, 4873; i) B. Adhikari, C. Singh, A. Shah, A. J. Lough, H.-B. Kraatz, *Chem. Eur. J.* **2015**, *21*, 11560.
- [33] a) L. Barišić, M. Dropučić, V. Rapić, H. Pritzkow, S. I. Kirin, N. Metzler-Nolte, *Chem. Commun.* **2004**, *17*, 2004; b) L. Barišić, M. Čakić, K. A. Mahmoud, Y.-N. Liu, H.-B. Kraatz, H. Pritzkow, S. I. Kirin, N. Metzler-Nolte, V. Rapić, *Chem. Eur. J.* **2006**, *12*, 4965; c) L. Barišić, V. Rapić, N. Metzler-Nolte, *Eur. J. Inorg. Chem.* **2006**, 4019; d) M. Čakić Semenčić, D. Siebler, K. Heinze, V. Rapić, *Organometallics* **2009**, *28*, 2028; e) M. Čakić Semenčić, K. Heinze, C. Förster, V. Rapić, *Eur. J. Inorg. Chem.* **2010**, 1089; f) J. Lapić, D. Siebler, K. Heinze, V. Rapić, *Eur. J. Inorg. Chem.* **2007**, *14*, 2014.
- [34] S. Chowdhury, K. A. Mahmoud, G. Schatte, H.-B. Kraatz, *Org. Biomol. Chem.* **2005**, *3*, 3018.
- [35] T. Moriuchi, T. Hirao, *Kobunshi Ronbunshu* **2016**, *73*, 1.
- [36] M. Kovačević, I. Kodrin, S. Roca, K. Molčanov, Y. Shen, B. Adhikari, H.-B. Kraatz, L. Barišić, *Chem. Eur. J.* **2017**, *23*, 1037.
- [37] T. Moriuchi, T. Nishiyama, M. Nobu, T. Hirao, *Chem. Eur. J.* **2017**, *23*, 12704.
- [38] a) A. Lataifeh, S. Beheshti, H.-B. Kraatz, *Eur. J. Inorg. Chem.* **2009**, 3205; b) T. Moriuchi, T. Hirao, *J. Inclusion Phenom. Macrocyclic Chem.* **2012**, *74*, 23.
- [39] V. Rapić, M. Kovačević, *Kem. Ind.* **2012**, *61*, 71.
- [40] M. Massimi, A. Tomassini, F. Sciubba, A. P. Sobolev, L. Conti Devirgiliis, A. Miccheli, *Biochim. Biophys. Acta* **2012**, *1820*, 1.
- [41] J. Das, S. Pany, A. Majhi, *Bioorg. Med. Chem.* **2011**, *19*, 5321.
- [42] F. Mazué, D. Colin, J. Gobbo, M. Wegner, A. Rescifina, C. Spatafora, D. Fasseur, D. Delmas, P. Meunier, C. Tringali, N. Latruffe, *Eur. J. Med. Chem.* **2010**, *45* 2972.
- [43] Q. Liu, C. T. Kim, Y. H. Jo, S. B. Kim, B. Y. Hwang, M. K. Lee, *Molecules* **2015**, *20*, 16933.
- [44] M. Chalal, D. Delmas, P. Meunier, N. Latruffe, D. Vervandier-Fasseur, *Molecules* **2014**, *19*, 7850.
- [45] V. Kovač, I. Kmetič, T. Murati, M. Miletić, L. Barišić, *Croat. Chem. Acta* **2016**, *89*, 339.
- [46] I. Held, P. von den Hoff, D. S. Stephenson, H. Zipse, *Adv. Synth. Catal.* **2008**, *350*, 1891.
- [47] a) J. Bouckaert, J. Berglund, M. Schembri, E. De Genst, L. Cools, M. Wuhler, C.-S. Hung, J. Pinkner, R. Slättegård, A. Zavalov, D. Choudhury, S. Langermann, S. J. Hultgren, L. Wyns, P. Klemm, S. Oscarson, S. D. Knight, H. De Greve, *Mol. Microbiol.* **2005**, *55*, 441; b) A. Wellens, C. Garofalo, H. Nguyen, N. Van Gerven, R. Slättegård, J.-P. Hernalsteens, L. Wyns, S. Oscarson, H. De Greve, S. Hultgren, J. Bouckaert, *PLoS ONE* **2008**, *3*, e2040.
- [48] V. Kovač, R. Ribić, V. Petrović Peroković, S. Tomić Pisarović, L. Barišić, *Appl. Organometal. Chem.* **2016**, *30*, 524.
- [49] E. Ko, J. Liu, K. Burgess, *Chem. Soc. Rev.* **2011**, *40*, 4411.
- [50] A. Giannis, T. Kolte, *Angew. Chem. Int. Ed. Engl.* **1993**, *32*, 1244.
- [51] P. Čudić, M. Stawikowski, *Methods Mol. Biol.* **2008**, *494*, 223.
- [52] J. M. Lozano, L. P. Lesmes, L. F. Carreño, G. M. Gallego, M. Elkin Patarroyo, *Molecules* **2010**, *15*, 8856.
- [53] P. Wipf, J. Xiao, C. R. J. Stephenson, *Chimia (Aarau)* **2009**, *63*, 764.
- [54] C. Z. Gómez-Castro, I. I. Padilla-Martínez, E. V. García-Báez, J. L. Castrejón-Flores, A. L. Peraza-Campos, F. J. Martínez-Martínez, *Molecules* **2014**, *19*, 14446.
- [55] X.-W. Li, Y.-J. Zheng, Y.-T. Li, Z.-Y. Wu, C.-W. Yan, *Eur. J. Med. Chem.* **2011**, *46*, 3851.
- [56] J. Jiao, M. Jiang, Y.-T. Li, Z.-Y. Wu, C.-W. Yan, *J. Biochem. Mol. Toxicol.* **2014**, *28*, 47.
- [57] K. Zheng, L. Jiang, Y.-T. Li, Z.-Y. Wu, C.-W. Yan, *RSC Adv.* **2015**, *5*, 51730.

- [58] N. Sunduru, M. Sharma, K. Srivastava, S. Rajakumar, S. K. Puri, J. K. Saxena, P. M. S. Chauhan, *Bioorg. Med. Chem.* **2009**, *17*, 6451.
- [59] K. O. Yerdelen, E. Tosun, *Med. Chem. Res.* **2015**, *24*, 588.
- [60] F. Currelia, Y. D. Kwon, H. Zhang, D. Scacalossi, D. S. Belov, A. A. Tikhonov, I. A. Andreev, A. Altieri, A. V. Kurkin, P. D. Kwong, A. K. Debnath, *J. Med. Chem.* **2015**, *58*, 6909.
- [61] S. M. Curtis, N. Le, F. W. Fowler, J. W. Lauher, *Cryst. Growth Des.* **2005**, *5*, 2313.
- [62] Z.-L. Liu, L.-Cun, D.-Z. Liao, Z.-H. Jiang, S.-P. Yan, *Cryst. Growth Des.* **2005**, *5*, 783.
- [63] a) J. Makarević, M. Jokić, L. Frkanec, V. Čaplar, N. Šijaković Vujičić, M. Žinić, *Beilstein J. Org. Chem.* **2010**, *6*, 945; b) L. Frkanec, M. Žinić, *Chem. Commun.* **2010**, *46*, 522; c) J. Makarević, M. Jokić, Z. Raza, V. Čaplar, D. Katalenić, Z. Štefanić, B. Kojić-Prodić, M. Žinić, *Croat. Chem. Acta* **2004**, *77*, 403; d) J. Makarević, M. Jokić, B. Perić, V. Tomišić, B. Kojić-Prodić, M. Žinić, *Chem. Eur. J.* **2001**, *7*, 3328.
- [64] E. F. Montero-Vázquez, F. J. Martínez-Martínez, I. I. Padilla-Martínez, M. A. Carvajal-García, J. Hernández-Díaz, *ARKIVOC* **2008**, 276.
- [65] I. L. Karle, D. Ranganathan, K. Shah, N. K. Vaish, *Int. J. Pept. Protein Res.* **1994**, *43*, 160.
- [66] S. Coe, J. J. Kane, T. L. Nguyen, L. M. Toledo, E. Wininger, F. W. Fowler, J. W. Lauher, *J. Am. Chem. Soc.* **1997**, *119*, 86.
- [67] V. Kovač, K. Radošević, A. Bebek, J. Makarević, Z. Štefanić, L. Barišić, M. Žinić, V. Rapić, *Appl. Organometal. Chem.* **2017**, *31*, e3653.
- [68] C. Tomasini, N. Castellucci, *Chem. Soc. Rev.* **2013**, *42*, 156.
- [69] E. J. Calabrese, L. A. Baldwin, *Annu. Rev. Pharmacol. Toxicol.* **2003**, *43*, 175.
- [70] M. P. Mattson, *Ageing Res. Rev.* **2008**, *7*, 1.
- [71] G. Vanhoof, F. Goossens, I. De Meester, D. Hendriks, S. Scharpé, *FASEB J.* **1995**, *9*, 736.
- [72] B. K. Kay, M. P. Williamson, M. Sudol, *FASEB J.* **2000**, *14*, 231.
- [73] A. Troganis, I. P. Gerothanassis, Z. Athanassiou, T. Mavromoustakos, G. E. Hawkes, C. Sakarellos, *Biopolymers* **2000**, *53*, 72.
- [74] M. Kovačević, K. Molčanov, K. Radošević, V. Gaurina Srček, S. Roca, A. Čače, L. Barišić, *Molecules.* **2014**, *19*, 12852.
- [75] L. Barišić, M. Kovačević, M. Mamić, I. Kodrin, Z. Mihalić, V. Rapić, *Eur. J. Inorg. Chem.* **2012**, *11*, 1810.
- [76] T. Hayashi, T. Asai, H. Ogoshi, *Tetrahedron Let.* **1997**, *38*, 3039.
- [77] M. Čakić Semenčić, V. Kovač, I. Kodrin, L. Barišić, V. Rapić, *Eur. J. Inorg. Chem.* **2015**, 112.
- [78] V. Kovač, M. Čakić Semenčić, I. Kodrin, S. Roca, V. Rapić, *Tetrahedron* **2013**, *69*, 10497.
- [79] M. Iqbal, P. Balaram, *J. Am. Chem. Soc.* **1981**, *103*, 5548.
- [80] Y. V. Venkatachalapathi, B. V. V. Prasad, P. Balaram, *Biochemistry* **1982**, *2*, 5502.
- [81] J. L. Jios, S. I. Kirin, N. N. Buceta, T. Weyhmuller, C. O. Della Vedova and N. Metzler-Nolte, *J. Organomet. Chem.* **2007**, *692*, 4209.
- [82] M. Čakić Semenčić, I. Kodrin, L. Barišić, M. Nuskol, A. Meden, *Eur. J. Inorg. Chem.* **2017**, 306.
- [83] M. Kovačević, I. Kodrin, M. Cetina, I. Kmetič, T. Murati, M. Čakić Semenčić, S. Roca, L. Barišić, *Dalton Trans.* **2015**, *44*, 16405.
- [84] M. Kovačević, V. Rapić, I. Lukač, K. Molčanov, I. Kodrin, L. Barišić, *J. Mol. Struct.* **2013**, *1048*, 349.